Developing a Robust Harvest for High Cell Density CHO Cell Culture

by
Nicole Ann Oliver
B.S., Biological Engineering, Northwestern University, 2014

Submitted to the MIT Sloan School of Management and the MIT Department of Biological Engineering in Partial Fulfilment of the Requirements for the degrees of

Master of Business Administration and Master of Science in Biological Engineering
in conjunction with the Leads of Global Operations Program at the

MASSACHUSETTS INSTITURE OF TECHNOLOGY
May 8, 2020

@ 2020 Nicole Oliver. All rights reserved

Signature of Author……
MIT Sloan School of Management
MIT Department of Biological Engineering
May 8, 2020

Certified by.....
Roy Welsch, Thesis Supervisor
Professor of Statistics and Management Science, MIT Sloan School of Management

Certified by.....
Douglas Lauffenburger, Thesis Supervisor
Ford Professor of Biological Engineering, Chemical Engineering, and Biology

Accepted by.....
Maura Herson, Assistant Dean, MBA Program
MIT Sloan School of Management

Accepted by.....
Katharina Ribbeck, Chair, Graduate Program Committee
Professor of Biological Engineering

Amgen Proprietary - Confidential

THIS PAGE IS INTENTIONALLY LEFT BLANK

Developing a Robust Harvest for High Cell Density CHO Cell Culture

by Nicole Oliver
B.S., Biomedical Engineering, Northwestern University, 2014

Submitted to the MIT Sloan School of Management and MIT biological Engineering on May 8, 2019, in partial fulfillment of the requirements for the degrees of Master of Business Administration and Master of Science in Biological Engineering

Abstract

The biotechnology industry relies on living organisms (e.g., mammalian cells) in the production of therapeutically beneficial products. Significant developments within the biotechnology industry have focused on maximizing the productivity of these living organisms. One such development is perfusion culture manufacturing, the continual addition of nutrients and removal of waste. Perfusion culture processes offer the potential of increased cell density compared to fed-batch, allowing for smaller facility footprints.

The high cell densities resulting from perfusion processes give rise to challenges when harvesting the product from cell culture. Many harvest technologies cannot support high cell densities because they would require large footprints and/or would result in low yields. Microfiltration-based tangential flow filtration (TFF) and alternating flow filtration (ATF) best support high cell densities by maintaining high product yield and a small-manufacturing footprint. However, ATF/TFF membranes readily foul (i.e., the deposition of particles within membrane pores or on the membrane surface), leading to variable product sieving.

The study sought to understand the impact of particle size on TFF fouling through a series of filtration experiments. Perfusion cell culture supernatant was fractionated by particle size and filtered using TFF under varying operating conditions. The resulting pressures and sieving were measured to quantify fouling and its consequences.

The results demonstrated that the degree of fouling is dependent on particle size. Generally, increasing the particle size is associated with increased fouling and decreased harvest yield (18.31% decreased in harvest yield per 1 μm increase in particle size). Particles less than 0.1 μm are an exception to the general rule: these particles exhibited significant fouling, suggesting that underlying particle chemistry also contributes to aggregation and fouling.

The findings support decreasing ‘problematic’ particle sizes – particles less than <0.1 μm and greater than 1 μm – to decrease fouling and increase harvest yield. Possible solutions to reduce such cell debris include engineering cells with higher viability, pre-filtering the feed solution, reducing shear from the pump, and shifting harvest earlier.

Amgen Proprietary - Confidential

THIS PAGE IS INTENTIONALLY LEFT BLANK

Acknowledgments

I want to first thank my MIT academic advisors, Douglas Lauffenburger and Roy Welsch, for their advice and mentorship throughout the project. I am privileged to have learned from them.

Second, I want to thank Amgen Inc. for providing the opportunity, resources, and support to work on such a challenging and exciting project. I especially want to thank my supervisors: Glen Bolton, Kyle McElearney, and Nick Marchand. Their advice and mentorship were essential to the success of the project.

I am also grateful for the support structure at Amgen Inc. I want to thank Dollie Grajczak, who ensured our experience was enriching and enjoyable from start to end. I also want to thank Aine Hanley, the LGO executive sponsor at Amgen Inc. Her active involvement in our projects and championship of the LGO program enhanced our internship experience. Finally, I would like to thank MIT LGO alumni at Amgen Inc., who went above-and-beyond in helping us navigate the internship.

Special thanks to my fellow off-cycle Amgen Inc. interns, Aaron Baskerville-Bridges, Or Dan, and Zoe Wolszon. They provided continuous feedback and insights and inspired me to become a better leader and professional. I cannot imagine doing this work without them.

I also want to thank the MIT LGO program. The program has been a life-changing experience because of the supportive staff and amazing students. I would like to especially thank Thomas Roemer, Patty Eames, Ted Equi, and Anna Voronova.

Finally, I want to thank my family and friends who have been immensely supportive throughout my time at MIT.

Amgen Proprietary - Confidential

THIS PAGE IS INTENTIONALLY LEFT BLANK

Table of Contents

List of Figures

List of Tables

List of Equations

THIS PAGE IS INTENTIONALLY LEFT BLANK

Chapter 1: Introduction

A. Project Motivation

Amgen is a leading biotechnology company that develops and produces medicines for patients with serious illnesses. Biotechnology "refers to the use of biological systems (e.g., cells or tissues) or biological molecules (e.g., antibodies) for/in the manufacture of commercial products" [1]. The application of biological processes has revolutionized industries, from agriculture to pharmaceuticals. With the advent of recombinant DNA and hybridoma technology in the 1980s, biopharmaceutical companies could produce therapeutic proteins and peptides that treated diseases that small molecules could not (e.g., insulin for diabetes).

Biological knowledge has only continued to expand, enabling further healthcare innovation and a rapid increase in the number of first-in-class and best-in-class therapies. With exponential biotechnological progress came exponential market growth: starting from modest beginnings in the mid-1980s, the industry is now valued at over $100 billion and is comprised of over 10,000 companies [1]. Though the biopharmaceutical industry is continuing to grow, the landscape is becoming increasingly competitive for individual firms as companies tackle more challenging, niche diseases. The average cost to develop a new product increased from $1.19 billion in 2010 to $2.17 billion in 2017 [2]. Concurrently, the rate of return on biopharmaceutical R&D investments decreased from 10.1% to 3.2% from 2010 to 2017 [2].

In an increasingly competitive market, Amgen recognizes manufacturing as a differentiating capability. Amgen invests heavily in advancing internal biomanufacturing capabilities to both increase production

capacity and reduce cost. From 2014 to 2018, Amgen surpassed its commitment to reducing its manufacturing footprint by 23% by implementing higher efficiency processes (i.e., "next-generation biomanufacturing") [3]. Next-generation biomanufacturing increases cell culture density in the production bioreactor and productivity (mg of product/L of culture), thereby increasing production capacity per batch. With improved capacity, Amgen is better able to deliver "the right drug to the right patient every time."

Next-generation biomanufacturing relies heavily on perfusion processes to cultivate denser and more productive cell cultures. Cell cultures are commonly grown using fed-batch or perfusion processes. Fed-batch culture adds nutrients in a base medium and replenishes nutrients at discrete points once they are depleted. Perfusion processes, in contrast, continuously circulates media, simultaneously removing waste and adding nutrients. The product is either harvested continuously or retained within the bioreactor until peak cell density is reached. Approximately five-times more product is produced per volume using perfusion processes compared to fed-batch processes. With greater volumetric productivity, a smaller manufacturing footprint is needed, thereby lowering capital expenditures. Furthermore, Pollock *et al.* estimated a 20% reduction in the cost of goods using perfusion processes [4].

The high cell densities resulting from perfusion processes give rise to challenges when harvesting the product from cell culture (henceforth known as "harvest"). Many harvest technologies used in fed-batch processes cannot support perfusion cultures with viable cell densities approaching 10^8 cells/mL and cell viabilities ranging from 50 to 80%. These technologies are not suited for high cell densities because they would require prohibitively large footprints (e.g., dead-end) and/or would result in prohibitively low yields (e.g., expanded bed chromatography). Microfiltration-based tangential flow filtration (TFF) and

alternating flow filtration (ATF) best support high cell densities by maintaining high product yield and a small-manufacturing footprint. TFF and ATF are forms of crossflow microfiltration, meaning the feed stream flows in parallel to a permeable membrane. The permeate stream containing the molecule of interest flows perpendicularly through the membrane, driven by transmembrane pressure.

The most significant challenge with TFF/ATF is fouling, the deposition of particles within membrane pores or on the membrane surface. Membrane fouling increases resistance to fluid flow, which manifests in an increase in transmembrane pressure (TMP) and/or a decrease in permeate flux. With lower permeate flux, product sieving decreases, leading to low product yields. TMP may also surpass operational limits, requiring filter change-out before harvest can proceed. Overall, fouling limits process robustness and increases manufacturing costs via inconsistent yields and/or filter change-out. Numerous factors influence fouling, including feed inputs (e.g., cell viability; cell culture additives), operational inputs (e.g., crossflow; permeate flux), and raw material inputs (e.g., fiber material; fiber porosity), but the interrelation between these factors is not well-understood. Hence, fouling remains an unsolved, challenging, and widespread problem.

B. Problem Statement

Cell culture with higher densities and/or lower viability has been empirically associated with greater fouling in ATF/TFF. Solutions with higher concentrations of cell debris have a greater propensity to attach to membranes and are associated with a more rapid decline in sieving [5]. In contrast, viable cells have been shown not to cause fouling [6]. The results invite the obvious question: why are cell debris associated with fouling? The answer to this question will enable process development scientists to develop solutions to reduce fouling from cell debris.

Concerning filtration efficiency, cell debris differs in size, shape, and chemistry, which may contribute to membrane fouling in ATF/TFF. Cell debris is composed of particles primarily ranging from <1 nm to 1000 nm, which may block or clog membrane pores of the same magnitude. The shape of the particles is also irregular; filters are typically rated for spherical particles, so irregular shapes may more readily enter and block membrane pores [7]. Finally, lysed cells (i.e., broken cell membrane) expose particles of varying zeta potential, such as DNA, that may more readily attach to the membrane surface. Literature does not elucidate the impact of cell debris shape, size, or chemistry on membrane fouling. Hence, we decided to investigate one of these elements: particle size. The other elements are out-of-scope but are opportunities for future work.

Previous studies often investigate one fouling factor without considering its dependency on other variables, which limits the utility of the findings. Varying particle size while holding other variables constant only reveals the impact of particle size for one condition. Thus, we chose to conduct a multivariate study, varying particle size along with membrane pore size and permeate flux. If fouling is dependent on particle size, membrane pore size will likely dictate which particle size causes fouling (e.g., small particles may not foul membrane with large pores). Numerous studies have also demonstrated the importance of flux on fouling [8][5].

To summarize, we decided to investigate the impact of particle size on fouling under varying TFF operating conditions (pore size, flux). Our investigation will address the following problems: 1) it will reveal the relationship between particle size and membrane fouling, which is currently unknown, and 2) it will be translatable across multiple operating conditions, unlike one-dimensional fouling studies.

C. Hypothesis Statement and Research Methodology

We hypothesized that: 1) the degree of fouling is dependent on particle size, and 2) for a given particle size fraction, the extent of fouling is impacted by pore size and/or flux. We tested our hypothesizes empirically. Cell culture supernatant was fractionated by particle size and then filtered using TFF while varying the permeate flux and filter pore size (**Table 1-1**). The resulting pressures and sieving were measured to quantify fouling and its consequences. The study was constructed as a fractional factorial experiment (i.e., design consist of a carefully chosen subset of the experimental runs) following Design of Experiment (DOE) principles. The design enabled us to discern the effect of each factor on fouling, as well as the effects of interactions between factors on fouling. Chapter 3 describes the experiment in further detail.

		Particle Sizes (μm)					
		<0.1	**0.1 – 0.22**	**0.22 – 0.45**	**0.45 – 0.65**	**0.65 – 1**	**0.65 – 5**
Operating Conditions	**High Flux, Large Pore Size**	X		X		X	X
	High Flux, Medium Pore Size		X		X	X	X
	High Flux, Small Pore Size	X	X	X	X		
	Moderate Flux, Large Pore Size		X	X	X		
	Moderate Flux, Medium Pore Size	X	X	X	X	X	X
	Moderate Flux, Small Pore Size	X	X			X	X
	Low Flux, Large Pore Size	X	X		X		X
	Low Flux, Medium Pore Size	X		X	X	X	
	Low Flux, Small Pore Size		X	X	X	X	X

Table 1-1. Operating Conditions. *Each particle size fraction was filtered under varying operating conditions – specifically, flux and filter pore size. The levels of each factor were as follows: particle size fraction – 6 levels; flux – 3 levels; and pore size – 3 levels. A fractional factorial design was conducted, with the runs selected designated by X. A subset of the selected runs was also replicated.*

D. Scope and Limitations

To conduct the study within the internship time constraints, the scope of work was limited in the following dimensions (**Figure 1-1**):

1) Harvest Technology: Crossflow microfiltration because it best supports high cell densities from perfusion processes while also maintaining a small manufacturing footprint.
2) Crossflow Mode: We focused on TFF for several reasons. First, TFF equipment supports membranes with small filtration areas, and thus TFF requires less feed material than ATF. Second, unidirectional flow is less complex to model than bidirectional flow. Hence, TFF is logically studied first; the ATF model can then be built upon the TFF model. Third, TFF equipment allows for higher crossflow rates than current ATF equipment, which enables conditions that may reduce fouling. For this reason, Amgen is exploring TFF as an alternative to ATF.
3) Membrane Type and Material: We limited the study to polysulfone (PS) hollow fiber membranes in alignment with Amgen protocol. PS is a standard membrane material for the biotechnology industry. Hollow fiber modules are used over cassettes because cassettes increase shear, which is thought to be harmful to cells.
4) Fouling Factors: Fouling factors we decided to investigate are particle size, pore size, and permeate flux (see **Appendix A**).

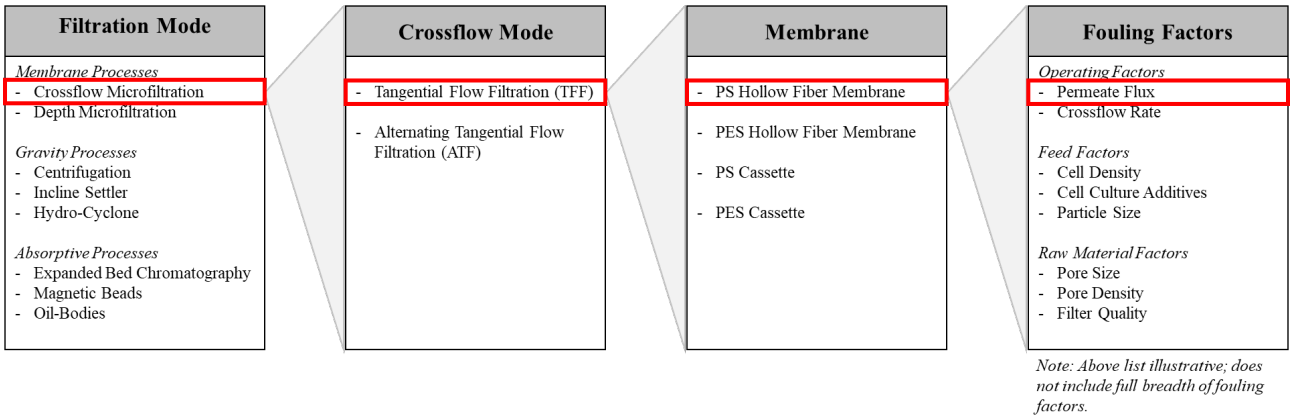

Figure 1-1. Scope of Work. *The schematic illustrates the scope of work. The scope of work was defined by sequentially selecting the filtration mode, crossflow mode, membrane, and fouling factors.*

E. Thesis Overview

The thesis is organized into five chapters. The first chapter introduced the project motivation and scope. The second chapter reviews the project background and relevant literature. The third chapter covers the experiment design and data analysis methodology. The fourth chapter discusses the project results. Finally, the fifth chapter reviews the project conclusions and next steps.

Chapter 2: Problem Background

A. Biomanufacturing

Biomanufacturing utilizes biological systems to produce therapeutically-important biomolecules, including monoclonal antibodies, peptides, and Car T cells. The biomanufacturing process is divided into upstream and downstream processes (**Figure 2-1**). During **upstream processing**, the cell line is grown to high densities in shake flasks and bioreactors of increasing volume to generate enough cell mass to inoculate the production bioreactor. Within the production bioreactor, cells are grown to even higher densities, after which the desired protein is harvested from the cell culture for downstream processing. During **downstream processing**, the therapeutic protein is purified (e.g., to remove cell debris, host-cell proteins, viruses, and non-native proteins) and the final product is formulated. The upstream and downstream processes are reviewed in further detail below.

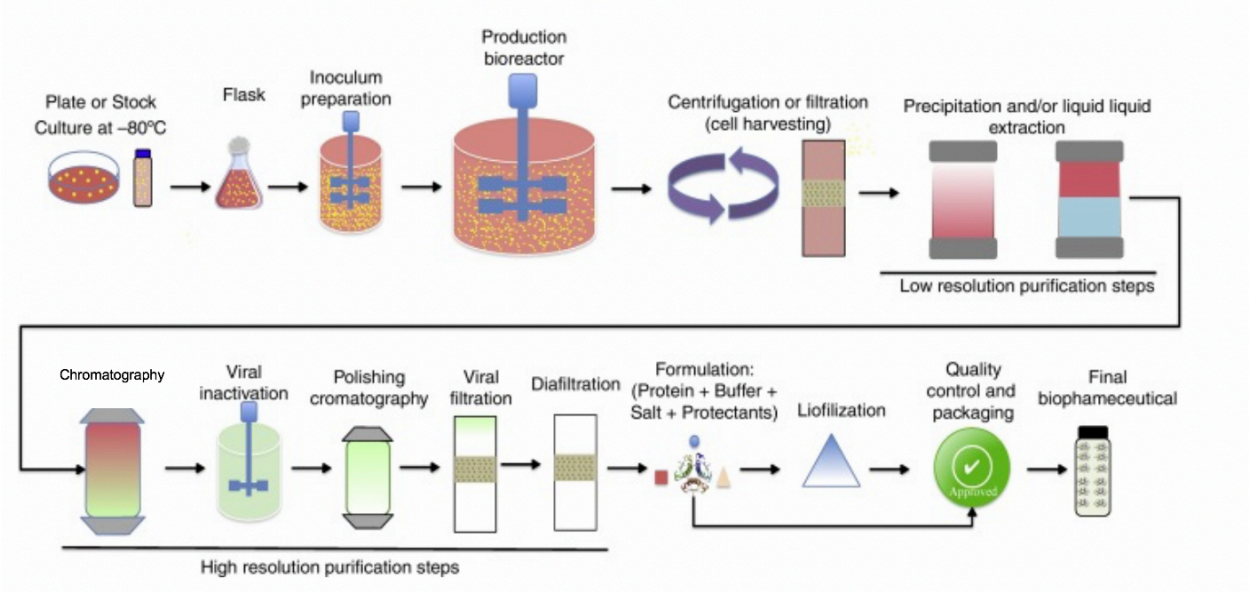

Figure 2-1. Biomanufacturing Process. *The schematic illustrates the biomanufacturing process. The upstream process includes the first step through harvest, while the downstream process includes all purification steps* [9].

i. Cell Line Development (Pre-Manufacturing)

Chinese Hamster Ovary (CHO) cell lines are the preferred expression platform for therapeutic proteins for several reasons. 1) CHO cells readily grow in suspension culture in serum-free media [10]. 2) They produce proteins similar to those produced in humans – i.e., complex proteins with post-translational modifications, including glycosylation. 3) CHO cells also secrete the final protein, eliminating the need to lyse the cells and subsequently refold the protein [11]. 4) Finally, few human viruses are able to grow within CHO cell culture. Because of their known safety profile, CHO cells require less regulatory effort compared to novel expression platforms.

Before clinical development, the cell line is developed and optimized for the production of the final product. A CHO cell lines is transfected with the genes necessary to produce the desired therapeutic protein. The transfected cells are cloned and expanded, and top clones are selected based on their product quality, yield, growth rate, and viability. The expansion and selection processes are repeated, ultimately narrowing the pool to the optimal cell line. The optimal cell line is cryopreserved in numerous vials or bags for commercial production. The cryopreserved vials/bags are known as the Master Cell Bank (MCB) – the initial therapeutic-producing cell line. From one vial of the MCB, several hundred Working Cell Banks (WCB) are produced. To initiate a manufacturing run, one vial of the WCB is thawed and propagated. The purpose of the MCB and WCB is to prevent genetic variation and potential contamination.

ii. Upstream Process

The upstream process is initiated by thawing one vial/bag from the Working Cell Bank – the vial/bag contains cells optimized to produce the desired therapeutic protein. The cells are propagated in a series of increasingly larger containers (e.g., T-flasks, shake flasks, small scale bioreactors). The purpose of the propagation process, also known as the seed train, is to generate an adequate number of cells for the inoculation of the production bioreactor [12]. After the production bioreactor is inoculated, the cell culture continues to grow, and the cells express the therapeutic protein. Finally, the therapeutic protein is separated from the cell culture using varying harvest technologies (**Chapter 2, Section C: Harvest Technologies**). Throughout the upstream process, the extracellular conditions – including pH, temperature, and nutrients – are regulated to maximize cellular growth and PQ.

iii. Downstream Process

The purpose of the downstream process is to purify the therapeutic protein. The downstream process can be divided into three stages. The **capture/recovery stage** immediately follows harvest. Though harvest partitions the product from cell culture, the harvest stream is contaminated with cell debris. The purpose of capture/recovery is to remove micron-sized particulate matter – including cell debris, growth media, and proteases – through depth filters or affinity chromatography resins. Post-capture/recovery, the stream is ~95% pure [13]. The **intermediate purification stage** follows capture/recovery and removes bulk containments, such as CHO proteins and viruses, most commonly using Protein A chromatography. Protein A, derived from *Staphylococcus auereus,* contains several domains that bind strongly with IgG and thus serve as highly-specific resins for IgG purification. Lastly, the **polishing stage(s)** removes any remaining impurities, including non-native forms of the protein. Common methods of capture,

purification, and polishing are reviewed in **Table 2-1** (from [13]). After downstream processing, the purified drug product is sterilely formulated, filled, and finished. The fill/finish process is essential to maintain product safety and stability (i.e., prevent protein denaturation).

Step	Method	Attributes	Benefits	Limitations
Capture	Chromatography	Protein A Affinity	High throughput High purity	High material cost
Capture	Chromatography	Other affinity ligands (e.g., Protein G)	High throughput	Purity Regulatory acceptance
Capture	Simultaneous clarificatio & capture	Cation exchange	Low cost media	Low throughput Preconditioning required
Capture	Simultaneous clarificatio & capture	Expanded bed adsorption (EBA)	Reduces unit operations	Sensitive to feed variatio & fouling
Purification	Chromatography	Ion exchange	Variety of selectivities High capacity & robust	Often flow rate limited
Purification	Adsorptive membrane	Charged membranes	High throughput containe trace contaminant remov	Low capacities

Table 2-1. Downstream Methods*. Various technologies are used to capture and purify the product, each with distinct advantages and disadvantages* [13].

B. Bioreactor Processes

The biomanufacturing process hinges on productive, high-cell density cell cultures. Cell culture processes have improved in reliability and robustness since the inception of the modern biotechnology industry. Numerous advancements have contributed to the maturity of cell culture processes, including sensors for process control, improved cell line engineering and selection, and optimized culture conditions [14]. Culture conditions, specifically the feed strategy within the production bioreactor, influence the harvest method and yield. The two-most dominant feed strategies are fed-batch and perfusion (**Figure 2-2**), each with notable advantages and disadvantages.

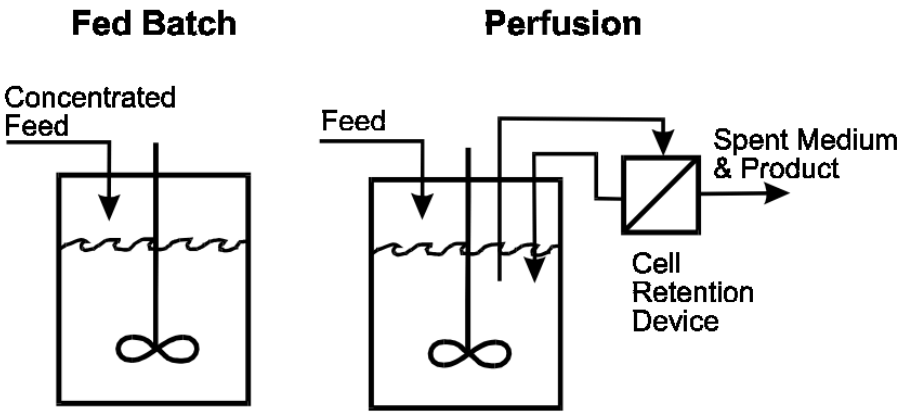

Figure 2-2. Fed-Batch vs. Perfusion Culture. *Fed-batch and perfusion are two widely used culture processes. Fed-batch adds feed in response to the depletion of one or more nutrients. Perfusion continuously replenishes nutrients and removes by-products* [15].

i. Fed-Batch

Fed-batch culture adds nutrients in a base medium and replenishes nutrients at discrete points once they are partially depleted (e.g., 50% depletion). The product is subsequently harvested from the culture and purified using one of various harvest technologies (see **Section C** below). Fed-batch is often used for production of biologics because it is reliable and simple – both in implementation and operation. Pollock *et al*. used stochastic processes to simulate both fed-batch and perfusion culture [4]. Based on the simulation results, they rated fed-batch and perfusion from 3 to 9 (3 = best, 9 = worst) on various attributes. Fed-batch received a rating of 3 for "ease of validation", "ease of development", and "ease of control/operation". Perfusion culture received ratings of 8, 7, and 8 for these attributes, respectively. Though fed-batch is simpler, it is not without disadvantages. Fed-batch culture continuously deteriorates because by-products are not removed. Thus, fed-batch culture cannot grow to the densities achieved using perfusion processes and is not suitable for unstable products.

ii. Perfusion Culture

In perfusion culture, fresh media is continuously supplied, and by-products are continuously removed. Thus, perfusion is preferred for the production of proteins that are unstable in the presence of toxic by-products. Moreover, with perfusion, higher cell densities are achieved compared to fed-batch – 30-100 x 10^6 cells/mL versus 5-25 x 10^6 cells/mL [16].As a result, perfusion increases the overall yield, thereby addressing capacity constraints. Finally, because of the increased productivity, a smaller manufacturing footprint is needed to produce large amounts of product. Thus, the capital costs to set-up a new line or plant are reduced, which allows for more flexibility in the manufacturing network.

Perfusion is operationally more complex than fed-batch because it necessitates a cell-retention device – a device that enables the exchange of metabolites without damaging the cells. Common cell-retention devices are crossflow membrane filters, spin-filters, inclined settlers, continuous centrifuges, and ultrasonic separators [15]. The reliability of the cell-retention device has historically been an obstacle to the adoption of perfusion processes. Common issues with cell-retention devices include:

- Non-alternating hollow-fiber crossflow filtration (i.e., tangential flow filtration, or TFF) clog at high-flux and cell density [15].
- Spin filters are also susceptible to clogging and are difficult to replace because the filter screen lies within the bioreactor [17].
- Inclined settlers are prone to cell adhesion, while vertical settlers are difficult to scale because the required area is proportional to the bioreactor volume [17].
- Centrifuges inflict significant shear stresses, which damage cells and lower overall viability [17].
- Ultrasonic separators are primarily used in small-scale operations and have yet to be successfully scaled [17].

Despite the notable challenges, the reliability of cell-retention devices has improved through iterations of the traditional designs and modulation of operating conditions. Most notably, alternating tangential flow filtration (ATF) reduces fouling compared to TFF. ATF has emerged as a favored cell-retention device because it possesses the benefits of TFF – scalability, repeatability, robustness – with the additional advantage of reduced fouling.

When comparing the economic feasibility of fed-batch and perfusion, all costs – including development, validation, and operation – need to be considered. Pollock *et al.* estimated the lifecycle costs of both fed-batch and perfusion [4]. They found that the initial capital expenditure was almost 50% lower for perfusion compared to fed-batch. Perfusion also had lower cost of goods per gram (COGS) (media, etc.) – $31/gram compared to $39/gram for fed-batch. The lower COGS was attributed to the "self-conditioning ability of cells and less bioreactor turnover" [17]. The self-conditioning ability of cells leads to increased secretion of growth factors at higher cell densities, which allows for a lower concentration of expensive media components [17]. However, fed-batch required less time and money in development and validation. Fed-batch was also superior when considering ease of control/operation and batch-to-batch variability [4]. Summing all costs, Pollock *et al.* calculated a 20% reduction in costs using perfusion compared to fed-batch. Their results are consistent with other studies – Shevitz *et al.* estimated a 45% to 20% reduction in costs using perfusion compared to fed-batch and concentrated fed-batch, respectively.

C. Harvest Technologies

Numerous methods are utilized to harvest the product from cell culture, including membrane processes, gravity processes, adsorptive processes, and phase-separation processes (**Table 2-2**).

Membrane Processes	Gravity Processes	Adsorptive Processes	Phase-Separation Process
Crossflow Microfiltration - ATF-XMF - TFF-XMF Depth Microfiltration Disposable Rotary Drum Filter	Centrifugation Inclined Settler Hydro-Cyclone	Expanded Bed Chromatograph Magnetic Beads Oil-Bodies Magnetite	Aqueous Two-Phase Extracti

Table 2-2. Harvest Technologies. *A variety of technologies are utilized to harvest product from cell culture, including membrane, gravity, adsorptive, and phase-separation processes.*

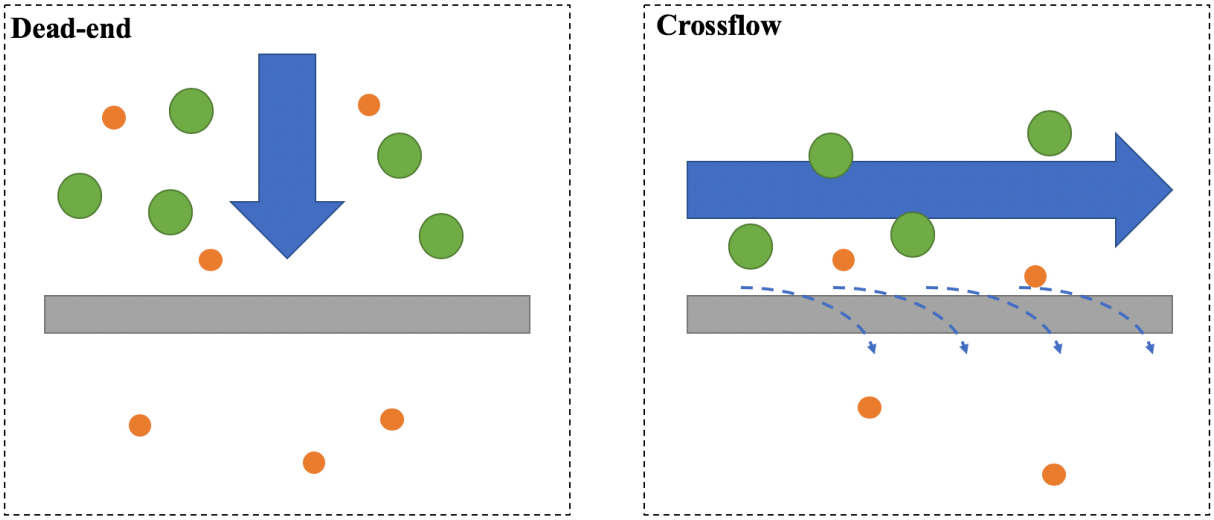

Figure 2-3. Dead-end vs. Crossflow. *In dead-end filtration, the fluid flows directly through the filter. In crossflow filtration, the filter flows parallel to the filter. Small particles permeate the filter driven by transmembrane pressure.*

Membrane processes use filters to separate the product from cell culture based on particle size exclusion. In depth-filtration, the cell culture flows directly through the filter (**Figure 2-3**). The product permeates the filter, while cells are excluded based on size. In contrast, in crossflow microfiltration (XMF), the cell culture flows parallel to the filter with micron-sized pores (**Figure 2-3**). The pressure in the outer lumen is greater than the pressure in the inner lumen, which drives the product through the filter. The cells are too large to permeate the filter and return to the bioreactor (the diameter of CHO cells is ~ 10 µm while the diameter of filter pore sizes is typically 30 kDa – 1 µm). Crossflow microfiltration reduces fouling compared to depth filtration because the parallel flow increases shear

forces at the membrane surface. Consequently, a lower filtration area is needed using crossflow mode compared to dead-end mode. Alternating tangential flow (ATF) and tangential flow filtration (TFF) are two modes of crossflow filtration. In TFF, the feed stream is unidirectional and orthogonal to the filter surface; in ATF, the feed stream alternates direction via a diaphragm pump (pressure, exhaust cycles) (**Figure 2-4**).

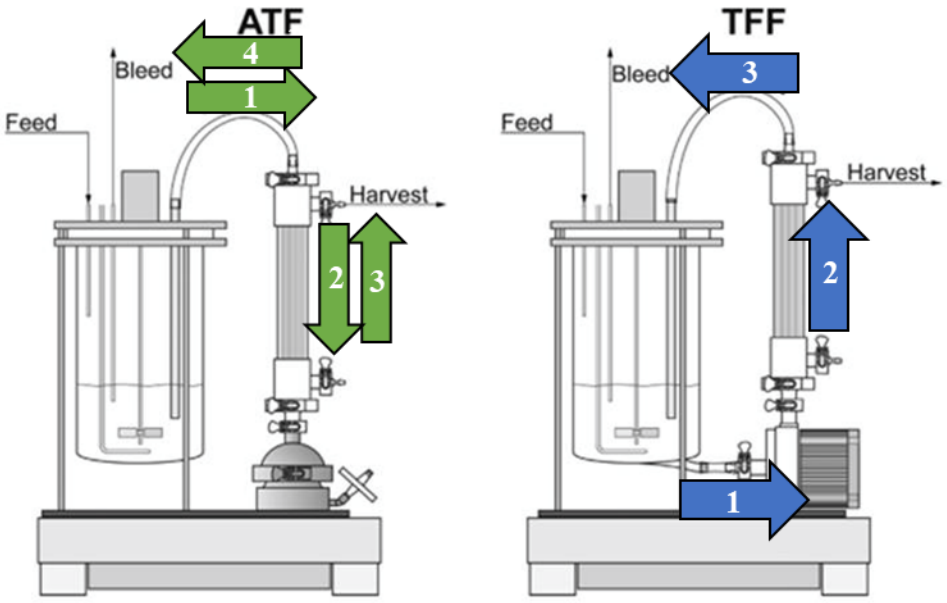

Figure 2-4. ATF and TFF. *In ATF, the feed stream alternates direction via a diaphragm pump (pressure, exhaust cycles), while in TFF the solution flows through the filter in a circular direction* [18].

Gravity processes separate based on sedimentation principles, which state that centrifugal acceleration causes denser particles to move outward compared to less dense particles. In centrifugation, the denser particles (e.g., cells) settle before the less dense particles (e.g., product). Centrifuges perform well with low-density cultures. However, the frequency of discharges (i.e., removal of settled matter) increases with cell density, which impacts yield and stresses the equipment. Continuous discharge alternatives are a promising alternative to alleviate problems with traditional centrifuges. Other methods relying on gravity processes include incline settlers and hydro-cyclones. All gravity processes improve after

chemical modifications – such as acid precipitation and flocculation. In acid precipitation, the pH is lowered to aggregate smaller cell debris to increase their sedimentation rate. Similarly, flocculants cause cell debris for improved separation.

Adsorptive processes rely on different absorption rates to separate product from cell culture. The most widely used absorptive process is expanded bed chromatography (EBA). The resin bed is first expanded by an upward flow of buffer [19]. The feed solution is then passed upward through the resin. The product is absorbed by the resin, while the remaining cell culture components are eluted. EBA is appropriate for cell cultures with high viability and low density. At high cell densities, cell debris clogs the resin, causing the expanded bed to collapse. Other adsorptive processes include magnetic beads and oil-bodies.

Lastly, **phase separation processes** separate the product from the culture after separating the mixture into distinct phases. In aqueous two-phase extraction, two polymers or a polymer and a salt are added to an aqueous solution. One polymer is covalently modified to attach an affinity ligand that binds to the final product [20]. In the aqueous solution, the polymer aggregates due to its hydrophobicity, thereby forming a distinct phase that contains the final product. However, the technology is still immature, and the partitioning is complex and not easily predicted [21].

For the remainder of the thesis, the focus is on ATF and TFF. Both technologies are widely used across the biotechnology industry because of their reliability and robustness.

D. Fouling Principles

Membrane fouling is the accumulation of particles on the membrane surface and/or the retention of particles within the membrane matrix or pores. Foulants are brought to the membrane by convective transport, which is the sum of diffusion, the random motion of individual particles in the fluid, and advection, the transport of matter by the larger-scale motion of currents [22][23]. In microfiltration-based TFF/ATF, particles are transported to the membrane via the orthogonal flow of fluid through the filter, driven by a pump or transmembrane pressure. Thus, the rate of fouling is dependent on permeate velocity.

At the membrane surface, the rejected particles either 1) dissolve and back-diffuse in the bulk fluid, or 2) remain non-dissolved and are absorbed by the membrane. The dissolved particles form a concentration polarization layer, while the absorbed particles act as foulants. Both concentration polarization and fouling increase resistance to solvent flow through the membrane and thus limit ATF/TFF efficiency [24][25][26].

i. Concentration Polarization

Concentration polarization is depicted in **Figure 2-5** [25]. Concentration polarization is a boundary layer containing a higher concentration of particles than the bulk. The layer is formed naturally by the selectivity of the membrane; as the membrane rejects particles, some particles back-diffuse, forming a region of higher concentration. The concentration polarization layer may cause a decline in permeate flux, even without fouling [25][27].

Although concentration polarization is distinct from fouling, the two phenomena are interrelated. Higher concentrations of particles at the membrane surface increase the probability of foulant adsorption,

thereby transitioning from concentration polarization to fouling [25][27]. By filtering fine silica colloids under controlled conditions, Chen *et al.* demonstrated that the polarized layer formed a cake structure (a type of fouling) above a critical flux [28]. The cake structure, evident via electron micrographs, caused an increase in TMP and a decrease in permeate flux. Inversely, reducing the concentration polarization layer minimizes the transition to irreversible fouling. Improved mass transfer, such as by increasing the crossflow rate, will reduce surface concentrations and thus fouling [25]. Chen *et al.* showed that increasing the crossflow rate effectively increased the critical flux at which the polarization layer transitioned to fouling [28].

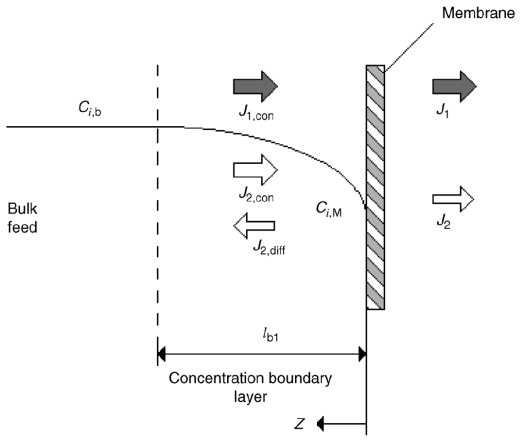

Figure 2-5. Concentration Polarization. *Concentration polarization is a boundary layer containing a higher concentration of particles than the bulk. The layer is formed naturally by the selectivity of the membrane; as the membrane rejects particles, some particles back-diffuse, forming a region of higher concentration* [25].

ii. Fouling

Fouling is categorized both by its reversibility and mechanism. Reversible fouling can be removed by physical means, such as reversing the flow of the feed-stream, while irreversible fouling can only be removed by chemical means [22]. Broadly, internal and external fouling are the primary fouling

mechanisms. Internal fouling is characterized by the build-up of foulants on pore walls and/or membrane fibers; external fouling characterized by the growth of a foulant layer on top of the membrane surface [29].

Internal fouling is further divided into different modes. There are three modes of internal fouling in membranes composed of straight, cylindrical pores (i.e., hollow fiber membranes): standard blocking, complete pore blockage, and intermediate pore blockage [30]. In **standard blocking** (also known as pore constriction), pores evenly decline in radius as foulants accumulate on pore walls [29]. Standard blocking increases resistance to fluid flow due to pore size reduction [25]. In **complete and intermediate blocking**, foulants block pore entrances completely and partially, respectively [29]. Both complete and intermediate blocking reduce the available filtration area. External fouling is synonymous with **cake fouling** or gel formation: all terms represent the deposition of particles on top of the membrane, essentially a secondary membrane. The fouling modes are depicted in **Figure 2-6**.

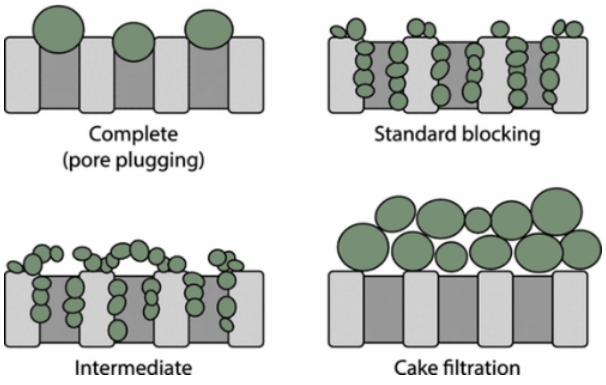

Figure 2-6. Fouling Modes. *There are four types of fouling – complete, standard blocking, intermediate, and caking. Complete and intermediate block the pore heads completely and partially, respectively. Standard blocking narrows the pores. Caking is the accumulation of particles on the membrane surface* [31].

All fouling mechanisms increase membrane resistance, i.e., the resistance to solvent flow through the membrane. Membrane resistance is calculated using Darcy's Law (**Eq. 2-1**):

$$J = \frac{TMP}{\mu(R_M + R_R + R_I)}$$

, where J is permeate flux $\left(\frac{m}{s}\right)$, TMP is transmembrane pressure $\left(\frac{kg}{m \cdot s^2}\right)$, μ is filtrate viscosity $\left(\frac{kg}{m \cdot s}\right)$, R_M (m^{-1}) is intrinsic membrane resistance, R_R (m^{-1}) is added resistance due to reversible fouling, and R_I (m^{-1}) is added resistance due to irreversible fouling [24]. Without fouling, the sole resistance is intrinsic (R_M) and permeate flux increases linearly with TMP. The flux-TMP curve begins to deviate from linearity with the onset of fouling. As shown by Darcy's Law fouling is detected by either an increase in TMP under constant flux operation or a decrease in permeate flux under constant pressure operation.

Fouling reduces harvest efficiency, increases production costs, and places an unnecessary burden on operators. Lower permeate flux due to fouling decreases product sieving for a given harvest cycle time. Reduced pore radius, specifically due to standard blocking, may also decrease sieving if the product can no longer permeate the pores. Harvest inefficiencies limit overall yield and production capacity – the product retained in the bioreactor (i.e., not harvested) cannot be recovered. Moreover, increased TMP due to fouling may surpass operational limits, halting the harvest process until the fouled filter is replaced. Filter change-out not only increases COGS but also increases the workload of operators.

E. Fouling Models

Hermia developed an equation that relates flux decline to fouling mode (**Eq. 2-2**):

$$\frac{d^2t}{dV^2} = k\left(\frac{dt}{dV}\right)^n$$

, where t is the filtration time, V is the volume filtered per unit area, and n is an index dependent on fouling mode [32]. A synonymous form of the equation calculates flux decline rather than the decline in volume filtered per unit time (**Eq. 2-3**):

$$\frac{dJ}{dt} = -kJ^{3-n}$$ [25].

In the second form of the equation, the impact of index n is apparent: the smaller the value of n, the greater the decline in permeate flux. The value of n depends on the fouling mode. n is equal to 0, 1, 1.5, and 2 for cake fouling, intermediate blocking, standard blocking, and complete blocking. Thus, cake fouling induces the steepest decrease in permeate flux under constant pressure.

Hernia's equation, though useful, was developed for dead-end filtration and is only valid for initial periods of crossflow filtration [25]. Hence, the equation is modified to include the effects of crossflow (**Eq. 2-4**):

$$\frac{dJ}{dt} = -k(J - J_{ss})J^{2-n}$$

, where J_{ss} is the steady-state flux [25]. Crossflow mediates fouling by shearing foulants from the membrane surface. The deposition of foulants via convection and the removal of foulants via crossflow eventually equalize, resulting in a non-zero steady-state flux [25].

F. Fouling Factors

Numerous factors influence fouling, from cell debris to filter porosity. The factors are often interrelated, making it difficult to distinguish individual effects. Fouling factors, and occasionally their interrelation, have been investigated extensively. The research is reviewed below, with factors organized into three categories: feed inputs (factors related to the feed stream), operational inputs (factors related to harvest

design and operation), raw material inputs (factors related to filter characteristics). **Table 2-3** summarizes the individual effects on fouling.

Category	Fouling Factor	Relationship with Fouling
Feed Inputs	Cell Culture Density	Higher density associated with more rapid fouling in TFF
	Cell Culture Viability	Lower viability associated with more rapid fouling
	Particle Size	Supernatant associated with fouling, independent of cell suspension
	Antifoam	Higher concentrations of antifoam associated with more rapid fouling
Operational Inputs	Mode (ATF, TFF)	ATF associated with less fouling because of the Starling Effect
	Crossflow Rate	Higher crossflow is associated with reduced fouling; however, excessive crossflow can negatively effect cell viability
	Permeate Flux	Higher flux associated with greater fouling
Raw Material Inputs	Filter Length	Shorter Filters associated with greater fouling
	Pore Size	Generally, larger pores associated with less fouling, but results have been mixed

Table 2-3. Fouling Factors. *The table summarizes the relationship between various filtration inputs and fouling.*

i. Feed Inputs

Feed inputs are factors related to cell culture within the production bioreactor. Given that there are 40 to 100 media components, cell culture is immensely variable in its formulation. Varying cell culture formulations result in different cell densities and viabilities, which impact downstream harvest.

Cell culture density is correlated with membrane fouling, with higher cell densities associated with rapid fouling of microfilters in both ATF and TFF mode. Researchers from Villanova University and Janssen Pharmaceuticals filtered mammalian cell culture with low and high densities (28*10^5 cells/mL

and 37*10^6 cells/mL, both with 91% cell viability) using ATF [5]. The high-density solution showed fouling within 320 minutes, while the low-density solution showed fouling within 430 minutes.

Similarly, Karst *et al.* filtered CHO cell culture of increasing densities (20, 40, and 60*10^6 cells/mL) using both ATF and TFF [18]. Instead of measuring direct indicators of fouling (i.e., membrane resistance, TMP, permeate flow), the authors measured a consequence of fouling – harvest yield. Interestingly, high yield (90%) was observed using ATF at all cell densities. High yield was also measured using TFF with low cell densities, but low yield (50%) was seen using TFF at high cell densities. The authors attribute that the difference in results is due to hydrodynamic differences between ATF and TFF: bidirectional flow in ATF causes back-washing, removing foulants (i.e., the Starling Effect).

While both studies suggest that higher cell densities are correlated with fouling, the ATF results illustrate the complexity of studying fouling. At approximately 40*10^6 cells/mL, Zhang *et al.* observed fouling while Karst *et al*. observed no sieving decline (suggesting minimal fouling). Variation in operating conditions between the two studies (i.e., crossflow rate, permeate flow rate, and filter length) could have contributed to observed differences, further illustrating the interdependency of fouling factors.

Cell viability, the percentage of live cells within the feed stream, has been shown to be negatively correlated within fouling. Cell death pathways include apoptosis and necrosis. Apoptosis is programmed cell death – it is a physiological process by which unwanted or useless cells are eliminated during the development and other normal biological processes. In contrast, necrosis is a pathological process that

occurs when cells are exposed to external triggers. In harvest, apoptotic triggers are dependent on bioreactor and ATF/TFF design. Media lot hold time and feed strategy affect nutrient availability, and ATF hold-up and poor mixing cause oxygen depletion.

Zhang *et al.* filtered solutions varying in cell viability using ATF and examined the membrane post-filtration using a scanning-electron microscope (SEM) [5]. The SEM analysis of the fouled membranes showed a cake layer containing cells. They found that low viability solutions led to greater "sticking" (i.e., cake layer formation). Lower viability cells not only attached more readily during the exhaust phase but also detached less readily during the pressure phase. The authors suggested that DNA, released during cell lysis, promoted cell adhesion to the membrane surface. Internal research also demonstrated that lower viability solutions resulted in a faster sieving decline, reaching the steady-state value within minutes.

The association of lower viability solutions with fouling brings about the following question: is cell debris contributing to fouling because of its size, chemistry, and/or shape? Work by Lin *et al.* supports further investigation into **particle size** [6]. They filtered three samples: material in the permeate stream (<10 nm), cell culture supernatant (<10 nm to >1 um), and cell pellet resuspended (> 1 um). Cell culture supernatant resulted in low sieving, while the other samples maintained high pass-through. Their work demonstrates that supernatant contributes to fouling, independent of cell suspension.

Previous work demonstrates that particle size is, at a minimum, a contributing factor to supernatant fouling. Duclos-Orsello *et al.* showed that particle size influences fouling mode [30]. They filtered three different solutions through 0.22 μm filters: 0.25 μm polystyrene microspheres, BSA solution, and a pre-

filtered BSA solution. The microspheres caused cake fouling because the microspheres were larger than the pores. The BSA solution caused pore blocking followed by caking; in contrast, the pre-filtered BSA solution caused minimal pore blocked and greater pore constriction because protein aggregates were removed.

Finally, the concentrations of **cell additives**, such as antifoam, are also correlated with fouling. Antifoam is added to cell culture to control foam and bubble formation. Zhang *et al.* demonstrated that antifoam adheres to membranes and causes fouling [5]. When filtering only media and antifoam (no cells), the membrane fouled within 12 minutes with an antifoam concentration of 4,500 ppm and within 8 minutes with an antifoam concentration of 6,000 ppm [5]. SEM images of membranes post-filtration indicated that antifoam micelles were deposited on the membrane (25 to 40 μm "hills" deposited on the membrane).

ii. Operational Inputs

Operational inputs are factors under-control by the process designer and harvest operator. Key operational inputs associated with fouling include mode (TFF, ATF), crossflow rate, permeate flux, and TMP.

TFF and ATF are both **modes** of crossflow filtration. ATF is theorized to out-perform TFF because of the Starling Effect. The Starling Effect is back-flux created by pressure gradients within the membrane. Throughout TFF and during the pressure cycle of ATF, the inner lumen (IL) pressure exceeds the permeate pressure, driving solute flow from the inner lumen to the outer shell. The pressure gradient is greatest at the inlet but gradually decreases along the fiber length. Close to the outlet (depending on fiber

length), the pressure gradient flips, and the permeate pressure exceeds the inner lumen pressure. This reverses the flow of fluid, creating a back-flux that cleans the membrane. In TFF, the back-flux only occurs at the far-end of the filter. However, because ATF alternates the direction of feed flow, the back-flux also alternates between the proximal and distal sections of the filter. Thus, a greater proportion of the membrane is cleaned in ATF.

Numerous studies cite the Starling Effect when explaining the performance differences between ATF and TFF. At high cell densities, Karst *et al.* measured high product yields (90%) using ATF but low product yields (50%) using TFF [18]. The authors attribute that the difference in results is due to hydrodynamic differences between ATF and TFF: bidirectional flow in ATF causes back-washing, removing foulants (i.e., the Starling Effect). Moreover, ATF resulted in lower hydrodynamic stress values than TFF with short, long, and no fibers [18]. The hydrodynamic stress is likely higher in TFF due to the larger effective cross-sectional area of the TFF pump compared to the ATF pump. In TFF, the hydrodynamic stress values readily exceed 32 Pa, the maximum stress tolerable by cells. Thus, the TFF pump may lower cell viability, which has been shown to contribute to fouling.

Karst *et al.* used a bearing-less centrifugal TFF pump in the previous study. Interestingly, when using the same pump, Coffman *et al.* found the performance comparable to ATF in both cell viability and product sieving [6]. They also compared the performance of TFF using a peristaltic pump. The peristaltic pump resulted in greater cell lysis, lower cell viability, and lower product sieving compared to the centrifugal pump. The results, specifically the lower cell viability, demonstrate the peristaltic pump is a major source of shear within the TFF system.

ATF is not without limitations. ATF has narrower operating ranges, given that it requires both vacuum and exhaust. Molleryd *et al.* compared cell culture densities used ATF and TFF; ATF and TFF were used to remove by-products of cell culture, not harvest product [33]. With ATF, the cell density peaked at 1.32*10^8 cells/mL. The cell density was limited by the vacuum capacity failing to pull the highly viscous cell broth. With TFF, the cell culture grew to higher densities (2.14*10^9 cells/mL), illustrating the potential of wider operating ranges.

Permeate flux is the volume flowing through the membrane per unit area per unit time ($m^3/m^2/s$). Permeate flux is typically controlled via a pump on the permeate line. Flux is linearly related to TMP through Darcy's Law (**Eq. 2-5**):

$$J = \frac{TMP}{\mu(R_M+R_R+R_I)}.$$

Because TMP drives particles to the membrane surface, higher flux increases the likelihood of fouling. The positive relationship between flux and fouling has been demonstrated repeatedly in literature. Internal research demonstrated that long-fibers exhibit minimal fouling at low fluxes, but rapid fouling at higher fluxes. The concept of "critical flux" has also been theorized – the hypothesis is that on start-up, there exists a flux below which minimal fouling occurs and above which fouling occurs. The critical flux depends on a variety of factors, including particle size. Gupta et al. estimated the critical flux values for particles ~0.1 μm to be 1-10 μm/s and particles ~ 1 μm to be 10 μm/s [8].

Crossflow is the flow rate of the feed solution through the filter (m/s). Generally, crossflow is thought to reduce fouling because it increases the shear forces at the membrane surface. However, the experimental results have not been conclusive. Bardliving *et al.* measured the membrane resistance after conducting filtration experiments using various crossflow rates. They found that both reversible and irreversible

membrane resistance was the highest for the membrane exposed to 0.70 m/s crossflow, followed by 0.22 m/s and 0.11 m/s [24]. In contrast, Lifia *et al.* found that raising the crossflow rate from 4 to 100 mm/s reduced the TMP from 59 to 24 kPa (suggesting a reduction in fouling) [34]. Together, the results suggest that increasing crossflow rates reduce fouling, but only below a certain threshold.

iii. Raw Material Inputs

In harvest, the primary raw material is the single-use filter. Filter attributes significantly impact fouling; key attributes include filter geometry (i.e., length, thickness), filter material, filter porosity (i.e., pore size, pore density), and filter quality.

Filter geometry, specifically shorter filters, is correlated with fouling. The Darcy-Weisbach equation (**Eq. 2-6**) describes the pressure drop across a pipe:

$$\Delta p = \frac{fL\rho v^2}{2D}$$

, where f is the friction factor, L is the pipe length, ρ fluid density, v is the fluid velocity, and D is the diameter. From **Eq. 2-6**, as the filter increases in length, the pressure drop increases proportionally. Thus, sufficiently long filters may have negative pressure toward the retentate end, meaning the pressure within the filter is less than the permeate pressure. The negative pressure causes the permeate to reverse direction (i.e., back-flushing), which cleans the membrane and reduces fouling.

Filter porosity encompasses numerous aspects, including pore size and pore density. Filters are rated on their ability to remove particles of a specific size through two methods: nominal and absolute rating [7]. The nominal rating indicates a filter's ability to reject a minimum percentage of particles greater than a

given micron size – e.g., 90% of 10 µm particles are rejected. Absolute rating, in contrast, indicates the diameter of the largest spherical particle that will pass through the filter in laboratory conditions – e.g., 10 um. The absolute rating is often considered unrealistic – operating pressure gradients are often higher than laboratory conditions; particles are often not spherical, etc.

Research related to pore size has yielded varying results. Stressmann *et al.* feed CHO cells through a TFF system under varying shear rates, controlled via feed pump speed [35]. Filters with small pores (0.2 µm) were associated with greater reversible and irreversible fouling at both low and high shear rates compared to filters with large pores (0.45 µm). Coffman *et al.* also demonstrated the benefit of larger pore sizes [36]. CHO cells were filtered using TFF with hollow fiber membranes of varying sizes and materials: 0.2 µm PES, 0.2 µm alpha-alumina, 5 µm alpha-alumina, and 2-10 µm PE (hollow fiber depth filter). The larger filters offered almost 100% product passage throughout the harvest cycle, while the 0.2 µm filters fouled within two days. No downstream impacts of the larger pore sizes were identified. Internal research, however, suggests that either small or large pore filters can be optimal depending on the accompanying set of conditions.

Filter quality also has an immense impact on fouling and product yield. A recent vendor change has reduced sieving and impacted yield.

Chapter 3: Materials and Methods

A. Experiment Overview

We hypothesized that: 1) the mode of fouling is dependent on particle size, and 2) for a given particle size fraction, the extent of fouling is impacted by pore size and/or flux. We tested our hypothesizes empirically. **First, CHO** cell culture supernatant, obtained via standard Amgen perfusion processes, was fractionated by size using dead-end and crossflow filtration. **Second,** each supernatant fraction was filtered using tangential flow filtration (TFF) under varying operating conditions (**Table 3-1**). The resulting pressures and sieving were measured to quantify fouling and its consequences. **Third**, polystyrene microspheres were filtered using TFF under a subset of the conditions. The microspheres were of similar diameter to the particles within the supernatant fractions. Comparing TMP and sieving curves of supernatant and microspheres revealed the relative impact of particle size versus chemistry. Note that all equipment used throughout the protocol is regularly maintained and calibrated by Amgen.

		Particle Sizes (μm)					
		<0.1	**0.1 – 0.22**	**0.22 – 0.45**	**0.45 – 0.65**	**0.65 – 1**	**0.65 – 5**
Operating Conditions	**High Flux, Large Pore Size**	X		X		X	X
	High Flux, Medium Pore Size		X		X	X	X
	High Flux, Small Pore Size	X	X	X	X		
	Moderate Flux, Large Pore Size		X	X	X		
	Moderate Flux, Medium Pore Size	X	X	X	X	X	X
	Moderate Flux, Small Pore Size	X	X			X	X
	Low Flux, Large Pore Size	X	X		X		X
	Low Flux, Medium Pore Size	X		X	X	X	
	Low Flux, Small Pore Size		X	X	X	X	X

Table 3-1. Operating Conditions. *Each particle size fraction was filtered under varying operating conditions – specifically, flux and filter pore size. The levels of each factor were as follows: particle size fraction – 6 levels; flux – 3 levels; and pore size – 3 levels. A fractional factorial design was conducted, with the runs selected designated by X. A subset of the selected runs was also replicated.*

B. Step 1: Separation of Cell Culture Supernatant by Size

To separate cell culture by particle size, whole cells were removed from cell culture to obtain supernatant (i.e., media and particulate matter) (**Centrifuge Cell Culture**). The supernatant was then fractionated by particle size using a combination of dead-end and crossflow filtration (**Fractionate Supernatant**). Finally, the size and concentration of the particles within each fraction were verified using dynamic light spectroscopy (DLS) (**Verify Particle Size Fractions**).

i. Centrifuge Cells

Two liters of CHO cell culture, grown via perfusion processes, were obtained from Amgen's Pilot Plant immediately following the production bioreactor step. Intact cells were removed via centrifugation (30 minutes at 3000 RPM), leaving only cell culture supernatant. The CHO cell culture was grown via standard Amgen protocol, so the particulate content in the supernatant was assumed to be representative of average batches. Thus, the study results are translatable to Amgen's production processes.

ii. Fractionate Supernatant

The cell culture supernatant was separated by particle size to generate six distinct bands: 1) 5-0.65 µm, 2) 1-0.65 µm, 3) 0.65-0.45 µm, 4) 0.45-0.22 µm, 5) 0.22-0.1 µm, and 6) <0.1 µm. To fractionate the supernatant, a combination of dead-end and crossflow filtration was utilized. Membrane filtration was

selected over centrifugation and chromatography because of equipment availability and volume constraints, respectively. Unlike the available centrifuge and resins, membrane filtration supported the large volume of supernatant, high particulate density, and micron and sub-micron particle sizes.

As illustrated in **Figure 3-1A and 3-1B**, the fractionation process involved two distinct filtration sequences: the first sequence generated Fraction 5-0.65 µm, while the second sequence generated the remaining fractions. Both sequences began with 1 L of supernatant with all particle sizes. The particles were then extracted from the supernatant bulk from largest to smallest using a series of filters with progressively smaller pore sizes. The filter separated the particles based on particle size, with particles less than the pore size flowing into the permeate and particles greater than the pore size flowing into the retentate. Thus, the permeate became the feed mixture for the next step while the retentate, bounded in size by the filters of the previous and current step, became Fraction *n*.

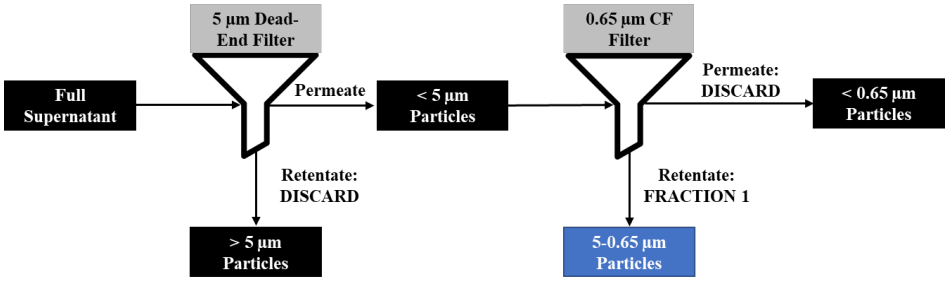

Figure 3-1A. Fractionation Line 1. *The 0.65-5 µm fraction was extracted using a dead-end filter with 5 µm pores and a crossflow filter with 0.65 µm pores. 1 L of the full supernatant was filtered using the dead-end filter, and the permeate was subsequently filtered using the crossflow filter. The resulting retentate contained particles bounded in size by both filters (i.e., 5-0.65 µm particles).*

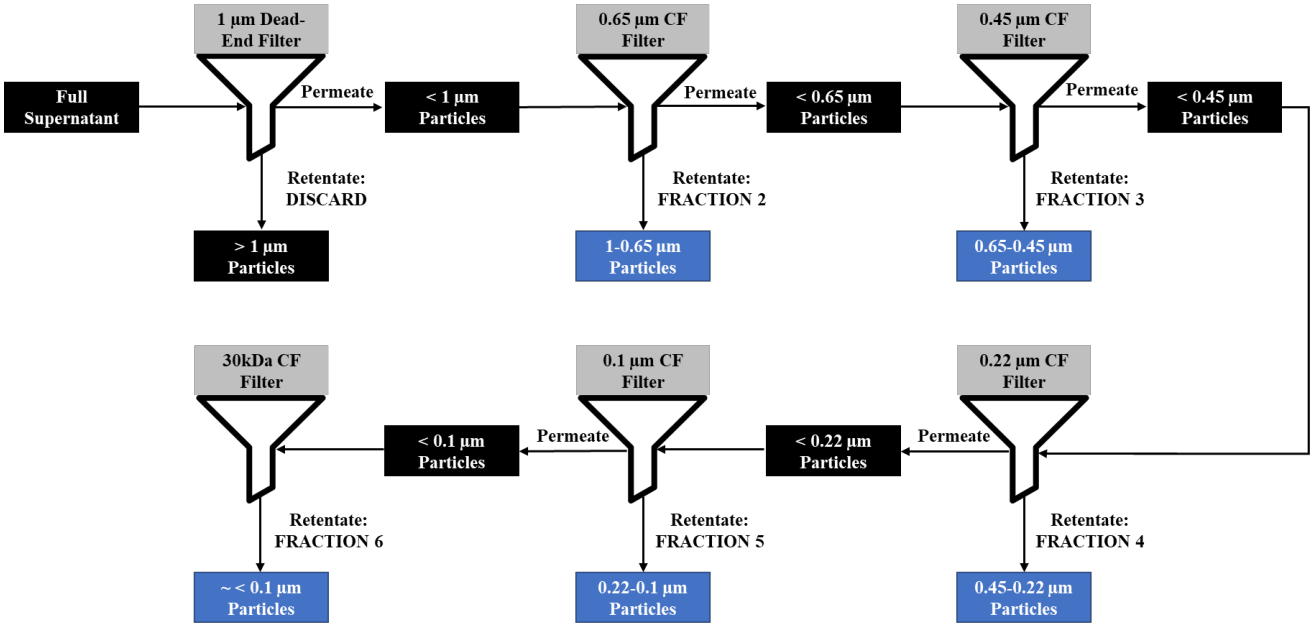

Figure 3-1B. Fractionation Line 2. *The second filtration sequence generated Fractions 2 through 6. The particles were then extracted from the supernatant bulk from largest to smallest using a series of filters with progressively smaller pore sizes.*

Dead-end Filter Procedure: The dead-end filters, manufactured by Whatman, were ordered in two pore sizes: 1 µm and 5 µm. Both dead-end filters encompassed a filtration area of 400 cm^2. The dead-end filter set-up is illustrated in **Figure 3-2**. The peristaltic pump drove the supernatant through the dead-end filter at 20 mL/min. A pressure sensor was placed after the peristaltic pump to ensure that the pressure remained below 15 psi, the maximum pressure tolerated by the tubing junctions. Particles smaller than the filter pore size permeated the membrane, while particles larger than the pore size returned to the main container. The permeate became the feed solution for the following crossflow filtration steps (see **Figure 3-1A and 3-1B**), and the retentate was discarded.

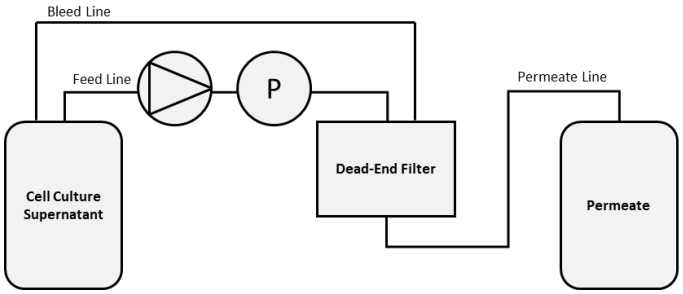

Figure 3-2. Dead-end Filter Set-up. *The schematic illustrates the dead-end filter set-up. The feed solution was pumped through the dead-end filter via a peristaltic pump. Particles smaller than the filter pore size flowed into the permeate, while the remaining particles returned to the main container.*

Crossflow Filter Procedure: The microfiltration cassettes, manufactured by Pellicon, were ordered in all available pore sizes: 30 kDa, 0.1 µm, 0.22 µm, 0.45 µm, and 0.65 µm. The filtration area for all cassettes was 0.1 m^2. The large filtration area was necessary to separate the supernatant effectively and efficiently. Fractionation was initially attempted with a smaller filtration area (50 cm^2). However, the filters readily fouled with the smaller filtration area, which restricted particle passage and increased the separation time.

The crossflow filter set-up is illustrated in **Figure 3-3.** The set-up relied on the PendoTech TFF Process Control System, which automatically controlled the feed flow rate and transmembrane pressure (TMP) based on pre-programmed values. The control system operated in three modes: concentration, diafiltration, and recovery. In concentration mode, the volume in the main container (i.e., feed solution) was reduced from its initial concentration to 0.5 L. The concentration step was necessary to minimize diafiltration time, which is a function of the main container volume. In diafiltration mode, particles were filtered by size – particles greater than the filter pore size returned to the main container, while particles less than the filter size entered the permeate. Finally, in recovery mode, PBS was added to the retentate

to recover the initial concentration and obtain Fraction *n*. For illustration, the extraction of the 1-0.65 µm fraction is described below:

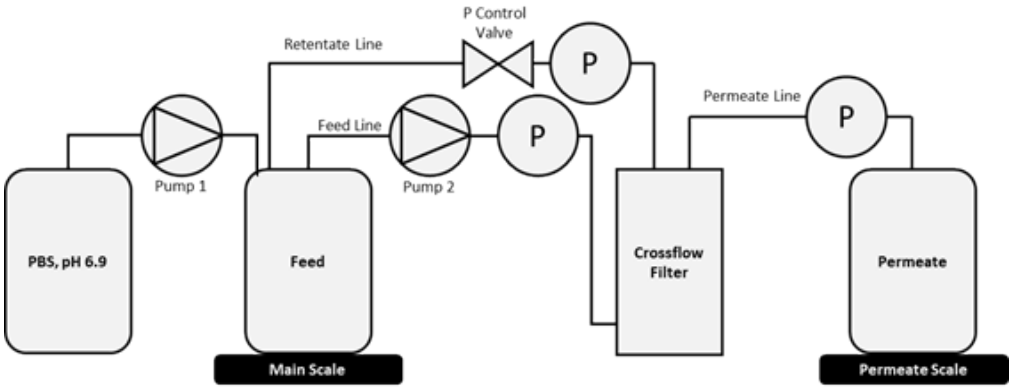

Figure 3-3. Crossflow Filter Set-up. *The schematic illustrates the crossflow filter set-up. The crossflow filter runs automatically via values pre-programmed into the PendoTech TFF Process Control System.*

- Concentration Mode:
    1. The feed solution was added to the main container. The feed solution was generated by the previous dead-end filtration step, which removed all particles greater than 1 µm. Thus, the main container contained 1 L of solution with particles < 1 µm.
    2. The following values were pre-programmed into the PendoTech TFF Process Control System: the circulation pump flow rate (20 ml/min), main scale end weight (500 mg), and TMP (15 psi).
    3. The system ran automatically based on the pre-programmed values. The circulation pump pumped the feed solution through the system at 20 mL/min, while the control valve regulated the retentate line pressure. Because of the control valve, the retentate line pressure was greater than the permeate line pressure (TMP = 15 psi). Thus, a portion of the feed solution flowed through the filter and entered the permeate.

4. The system stopped running once the main scale read 500 mg. Post-concentration, the main container contained 0.5 L (~500 mg) of solution with 2X the initial particle concentration, and the permeate container contained 0.5 L of solution with negligible particle concentration.

- Diafiltration Mode:
    1. Diafiltration immediately followed the concentration step. Thus, upon starting diafiltration, the main container contained 0.5 L of solution with 2X the initial particle concentration, and the permeate container contained 0.5 L of solution with negligible particle concentration.
    2. The following values were pre-programmed into the PendoTech TFF Process Control System: the peristaltic pump flow rate (20 ml/min), circulation pump flow rate (20 ml/min), permeate scale end weight (3000 mg), and TMP (15 psi). Note that the permeate scale end weight was set to six times the initial main scale weight (500 mg X 6) because six-volume exchanges are commonly considered necessary for complete filtration (i.e., to ensure that all particles smaller than the filter pore size enter the permeate).
    3. Again, the system ran automatically based on the pre-programmed values. The circulation pump pumped the feed solution through the system, while the control valve regulated the retentate pressure to maintain a pressure differential across the membrane. Driven by TMP, particles less than the filter pore size passed through the filter and entered the permeate while all other components returned to the main container. Unlike during concentration, the main container weight remained constant by the influx of PBS, which offset weight loss to permeate.

4. After six volume exchanges (i.e., after the permeate scale reads 3000 mg), all particles less than the filter pore size were assumed to be in the permeate. The permeate became the feed solution for the next extraction (0.65-0.45 μm), and the retentate entered the final recovery step.

- Recovery Mode:
    1. Post-diafiltration, the main container contained the retentate – a solution with all particles between 1 and 0.65 μm at 2X the initial concentration. That is, if the full supernatant contained 1e9 particles per mL of 1 to 0.65 μm particles, then the retentate contained 2e9 particles per mL. The purpose of the recovery step was to return the solution to its initial concentration by adding 0.5 L of PBS.
    2. The following values were pre-programmed into the PendoTech TFF Process Control System: the peristaltic pump flow rate (20 ml/min) and the main scale end weight (1000 mg).
    3. The system ran according to these values – pumping PBS into the main container at 20 mL/min until the main scale read 1000 mg (~1 L). The final solution contained all particles between 1 and 0.65 μm at the same concentration as they appeared in the full supernatant.

The remaining fractions were extracted in the same manner, as outlined in **Table 3-2**. Post-extraction, each fraction was frozen in 80 mL aliquots at -70°C until filtration (**Chapter 3, Section C**). There was initial concern about the impact of the freeze-thaw cycle on the particulate content. However, internal research demonstrated that the freeze-thaw cycle does not significantly impact the concentration of particles within the supernatant (a.k.a. centrate) (**Figure 3-4**).

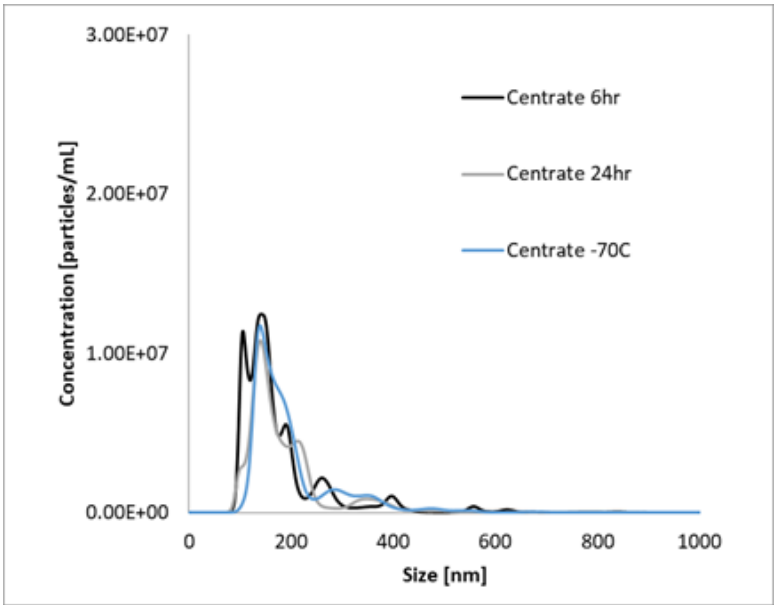

Figure 3-4. Freeze-Thaw Cycle. *The concentration and size of particles within supernatant were measured before freezing (Centrate 6hr, Centrate 24hr) and after freezing at -70°C (Centrate -70). The freeze-thaw cycle did not significantly impact the concentration or size of particles within the supernatant.*

Line 2			**Concentration**		**Diafiltration**		**Recovery**	
Step	**Pore Size**	**Main Vessel Start**	**Main Vessel End**	**Permeate End**	**Main Vessel End**	**Permeate End**	**Main Vessel End**	**Permeate End**
1	Dead-end 1 µm	Full solution (1 L) 1 X conc. All particles	N/A	N/A	Minimal - Disca 1 X conc. > 1 µm	1 L 1 X conc. < 1 µm	N/A	N/A
2	Crossflow 0.65 µm	Step 1 permeate (1 L) 1 X conc. < 1 µm	0.5 L 2 X conc. < 1 µm	0.5 L	0.5 L 2 X conc. 0.65-1 µm	3.5 L 1/3.5 X conc. < 0.65 µm	Fraction 2 (1 L) 1 X conc. 0.65-1 µm	3.5 L 1/3.5 X conc. < 0.65 µm
3	Crossflow 0.45 µm	Step 2 permeate (3.5 L) 1/3.5 X conc. < 0.65 µm	0.5 L 2 X conc. < 0.65 µm	3 L	0.5 L 2 X conc. 0.45-0.65 µm	6 L 1/6 X conc. < 0.45 µm	Fraction 3 (1 L) 1 X conc. 0.45-0.65 µm	6 L 1/6 X conc. < 0.45 µm
4	Crossflow 0.22 µm	Step 3 permeate (6 L) 1/6 X conc. < 0.45 µm	0.5 L 2 X conc. < 0.45 µm	5.5 L	0.5 L 2 X conc. 0.22-0.45 µm	8.5 L 1/8.5 X conc. < 0.22 µm	Fraction 4 (1 L) 1 X conc. 0.22-0.45 µm	8.5 L 1/8.5 X conc. < 0.22 µm
5	Crossflow 0.1 µm	Step 4 permeate (8.5 L) 1/8.5 X conc. < 0.22 µm	0.5 L 2 X conc. < 0.22 µm	8 L	0.5 L 2 X conc. 0.1-0.22µm	11 L 1/11 X conc. < 0.1 µm	Fraction 5 (1 L) 1 X conc. 0.1-0.22 µm	11 L 1/11 X conc. < 0.1 µm
6	Crossflow 30 kDa	Step 5 permeate (11 L) 1/11 X conc. < 0.1 µm	Fraction 6 (1 L) 1 X conc. < 0.1 µm	10 L - Discard	N/A	N/A	N/A	N/A

Line 1			**Concentration**		**Diafiltration**		**Recover**	
Step	**Pore Size**	**Main Vessel Start**	**Main Vessel End**	**Permeate End**	**Main Vessel End**	**Permeate End**	**Main Vessel End**	**Permeate End**
1	Dead-end 5 µm	Full solution (1 L) 1 X conc. All particles	N/A	N/A	Minimal - Disca 1 X conc. > 5 µm	1 L 1 X conc. < 5 µm	N/A	N/A
2	Crossflow 0.65 µm	Step 7 permeate (1 L) 1 X conc. < 5 µm	0.5 L 2 X conc. < 5 µm	0.5 L	0.5 L 2 X conc. 0.65-5 µm	3.5 L 1/3.5 X conc. < 0.65 µm	Fraction 1 (1 L) 1 X conc. 0.65-5 µm	3.5 L - Discard 1/3.5 X conc. < 0.65 µm

Table 3-2. Separation of Cell Culture Supernatant. *The table outlines the detailed protocol to generate the particle size fractions. The procedure involves concentrating the feed solution, filtering based on particle size, and recovering the initial concentration.*

iii. Verify Particle Size Fractions

After separation, the size distribution of the particles within each fraction was verified using Dynamic Light Scattering (DLS). DLS requires a monochromatic light source, usually a laser, which passes through a polarizer into the sample. Particles within the sample scatter the light, which is collected through a second polarizer. The resulting image is known as a speckle pattern – constructive interference of the scattered light appears light while destructive interference appears dark. New speckle patterns, as measured by light intensity changes, are generated as the particles move randomly through the solution (i.e., Brownian motion). Thus, the intensity fluctuations contain time-scale information about particle motion.

The dynamic information of particles in contained within the autocorrelation function, $g^2(q:x) = \frac{I(t)\cdot I(t+x)}{I(t)^2}$, where q is the wave vector, x is the time delay, and I is the intensity. At short time delays, the correlation is high because particles will not have moved far from their initial state. At long time delays, the correlation decays exponentially – to the point where there is no correlation between the scattered intensity of the initial and final states. The exponential decays are dependent on the motion of the particles, which is dictated by the diffusion coefficient. The diffusion coefficient is used to calculate the radii of the particles using the Stokes-Einstein equation.

Wyatt developed and manufactured the DLS equipment used in this experiment (**Figure 3-5**). The equipment includes hardware and software components, called the "DynaPro NanoStar" and

"DYNAMICS" respectively. The hardware includes a sample cell, laser, and detector; the software includes a user interface to run samples and view results. Operating the DLS equipment is straightforward: the sample (20 µL) is pipetted into a cuvette, which is placed within the sample cell of the DynaPro NanoStar. The laser illuminates the sample, and the scattered light is collected and correlated by the DynaPro NanoStar. Finally, the data is analyzed by the DYNAMICS software to calculate the hydrodynamic radii of the particles within the sample.

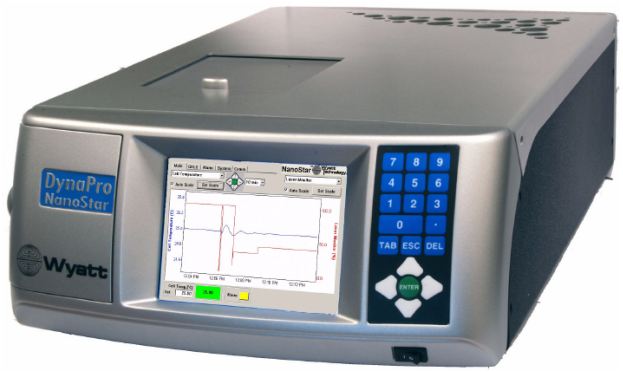

Figure 3-5. DynaPro NanoStar. *DynaPro NanoStar is a dynamic light scattering (DLS) machine that was used to measure the size of particles within each fraction.*

C. Step 2: Filter Supernatant Fractions Under Varying Conditions

The output of the fractionation process (Chapter C, Section B) was six fractions of cell culture supernatant, with each fraction containing distinct particle sizes. Next, each fraction was filtered using tangential flow filtration (TFF) under varying operating conditions. For each run, the extent of fouling was quantified by measuring the transmembrane pressure (TMP) and sieving (i.e., product passage). The filtration process represented the bulk of the empirical work and is described in detail through the following sub-sections:

1. Design of Experiment (DOE)

2. Overall Set-up
3. Materials and Equipment
4. Detailed Protocol

i. Design of Experiment (DOE)

The output of the fractionation process (Step 1) was six fractions of cell culture supernatant, with each fraction containing distinct particle sizes. Next, each fraction was filtered using tangential flow filtration (TFF) under varying operating conditions (**Table 3-3**). With six particle size fractions and nine operating conditions, a full factorial design yields 54 filtration runs. The number of experiments was reduced using Design of Experiment (DOE) principles to fit the experimentation duration within the internship timeline.

		Particle Sizes (μm)					
		<0.1	**0.1 – 0.22**	**0.22 – 0.45**	**0.45 – 0.65**	**0.65 – 1**	**0.65 – 5**
Operating Conditions	**High Flux, Large Pore Size**	X		X		X	X
	High Flux, Medium Pore Size		X		X	X	X
	High Flux, Small Pore Size	X	X	X	X		
	Moderate Flux, Large Pore Size		X	X	X		
	Moderate Flux, Medium Pore Size	X	X	X	X	X	X
	Moderate Flux, Small Pore Size	X	X			X	X
	Low Flux, Large Pore Size	X	X		X		X
	Low Flux, Medium Pore Size	X		X	X	X	
	Low Flux, Small Pore Size		X	X	X	X	X

Table 3-3. Operating Conditions. *Each particle size fraction was filtered under varying operating conditions – specifically, flux and filter pore size. The levels of each factor were as follows: particle size fraction – 6 levels; flux – 3 levels; and pore size – 3 levels. A fractional factorial design was conducted, with the runs selected designated by X. A subset of the selected runs was also replicated.*

A D-optimal design using JMP (statistics software) was utilized because standard 2-level and 3-level designs are not efficient given that the particle size fraction has six levels. That is, standard designs would require more experiments than could be completed within the internship timeframe. D-optimal designs are computer-generated designs constructed to minimize the variance of the regression coefficients by maximizing the determinant of X'X, where X is a matrix containing the independent variables [37]. Let $Xb = Y$ represent the system of equations, where X is a matrix containing the selected combinations of the independent variables, b is a vector containing the estimated coefficients, and Y is the response variable. The vector of coefficients is estimated by minimizing the sum of the square residuals $b = (X'X)^{-1}X'y$, and the 95% confidence interval is calculated by $\pm sqrt[(X'X)^{-1}] \cdot SD \cdot t - val$. It follows that maximizing X'X will minimize the confidence interval of the coefficients (i.e., maximize the precision).

To generate the D-optimal design specific to this study, the first step was to build a mathematical model describing the relationship between the independent variables (pore size, flux, and particle size) and the response (fouling). Interaction terms were included in the model because, as stated in the hypothesis, the impact of flux and pore size is presumed to be dependent on the particle size fraction (**Eq. 2-7**). Second and higher order interactions were excluded to limit experimental runs given the time frame allotted.

$$A \cdot Pore\ Size + B \cdot Flux + C \cdot Particle\ Size + D \cdot Pore\ Size \cdot Flux + E \cdot Pore\ Size \cdot Particle\ Size + F \cdot Flux \cdot Particle\ Size + G = Response$$

Next, a candidate set of points for the independent variables was outlined (matrix X). The candidate set of points represents the full factorial design, where every possible combination of the three variables is included (**Table 3-4A**). Finally, a subset of the candidate points was selected by the computer program (i.e., JMP) to maximize the determinant of the X'X matrix. The subset of candidates spanned the largest

possible volume of the experimental region. The resulting DOE included thirty-six unique runs and four replications (**Table 3-4B**). After generating the DOE, the runs were randomized by JMP to eliminate variability due to the learning curve of setting-up and running the experiments.

FULL FACTORIAL (MATRIX X)							
Run	Pore Size	Flux	Particle Size (um)	Run	Pore Size	Flux	Particle Size (um)
1	Large	High	<0.1	28	Large	High	0.45-0.65
2	Large	Moderate	<0.1	29	Large	Moderate	0.45-0.65
3	Large	Low	<0.1	30	Large	Low	0.45-0.65
4	Medium	High	<0.1	31	Medium	High	0.45-0.65
5	Medium	Moderate	<0.1	32	Medium	Moderate	0.45-0.65
6	Medium	Low	<0.1	33	Medium	Low	0.45-0.65
7	Small	High	<0.1	34	Small	High	0.45-0.65
8	Small	Moderate	<0.1	35	Small	Moderate	0.45-0.65
9	Small	Low	<0.1	36	Small	Low	0.45-0.65
10	Large	High	0.1-0.22	37	Large	High	0.65-1
11	Large	Moderate	0.1-0.22	38	Large	Moderate	0.65-1
12	Large	Low	0.1-0.22	39	Large	Low	0.65-1
13	Medium	High	0.1-0.22	40	Medium	High	0.65-1
14	Medium	Moderate	0.1-0.22	41	Medium	Moderate	0.65-1
15	Medium	Low	0.1-0.22	42	Medium	Low	0.65-1
16	Small	High	0.1-0.22	43	Small	High	0.65-1
17	Small	Moderate	0.1-0.22	44	Small	Moderate	0.65-1
18	Small	Low	0.1-0.22	45	Small	Low	0.65-1
19	Large	High	0.22-0.45	46	Large	High	0.65-5
20	Large	Moderate	0.22-0.45	47	Large	Moderate	0.65-5
21	Large	Low	0.22-0.45	48	Large	Low	0.65-5
22	Medium	High	0.22-0.45	49	Medium	High	0.65-5
23	Medium	Moderate	0.22-0.45	50	Medium	Moderate	0.65-5
24	Medium	Low	0.22-0.45	51	Medium	Low	0.65-5
25	Small	High	0.22-0.45	52	Small	High	0.65-5
26	Small	Moderate	0.22-0.45	53	Small	Moderate	0.65-5
27	Small	Low	0.22-0.45	54	Small	Low	0.65-5

Table 3-4A. Full Factorial*. The full factorial (left table) includes every possible combination of the three independent variables (6 X 3 X 3 = 54 runs).*

FINAL DOE							
Run	Pore Size	Flux	Particle Size (um)	Run	Pore Size	Flux	Particle Size (um)
1	Medium	Moderate	0.1-0.22	28	Medium	Low	0.65-1
2	Large	High	<0.1	29	Small	High	0.1-0.22
3	Large	High	0.22-0.45	30	Medium	High	0.45-0.65
4	Large	Moderate	0.45-0.65	31	Large	Low	0.45-0.65
5	Medium	Moderate	0.22-0.45	32	Small	High	<0.1
6	Small	Moderate	0.65-5	33	Large	High	0.65-5
7	Medium	High	0.1-0.22	34	Medium	Low	0.22-0.45
8	Medium	Moderate	0.65-5	35	Large	Low	0.65-5
9	Medium	Low	0.22-0.45	36	Small	Low	0.45-0.65
10	Small	Moderate	<0.1	37	Large	High	0.65-1
11	Medium	High	0.65-5	38	Small	Low	0.65-1
12	Large	Low	0.1-0.22	39	Small	Low	0.1-0.22
13	Medium	High	0.65-5	40	Small	Low	0.65-5
14	Large	Moderate	0.65-1				
15	Small	High	0.22-0.45				
16	Medium	Low	0.45-0.65				
17	Medium	Moderate	<0.1				
18	Medium	Moderate	0.45-0.65				
19	Medium	Low	<0.1				
20	Large	Moderate	0.1-0.22				
21	Small	Low	0.22-0.45				
22	Large	Moderate	0.22-0.45				
23	Medium	High	0.65-1				
24	Small	Moderate	0.1-0.22				
25	Large	Low	<0.1				
26	Small	High	0.45-0.65				
27	Small	Moderate	0.65-1				

Table 3-4B. Final DOE*. The full factorial was reduced to 40 runs (right table) by selecting the subset of runs that maximize the determinant of the X'X matrix.*

ii. Overall Set-up

The duration of each filtration run was three days to mimic a typical harvest cycle. The filtration set-up is shown in **Figure 3-6**. The particle size fraction was added to the main container, along with antibiotics and drug substance (DS). The solution within the main container flowed through the filter, driven by the bearingless pump. DS and other solution components smaller than the membrane pore size passed through the filter at a rate determined by the peristaltic pump. Any material that could not permeate the filter returned to the main container via the retentate line. Pressure sensors were added on the feed line, retentate line, and permeate line, which enabled the continuous measurement of TMP. The permeate and main container samples were obtained daily via Sample Port 1 and Sample Port 2. The titer (i.e., antibody concentration) within both samples were then measured using the Cedex Bio HT Equipment.

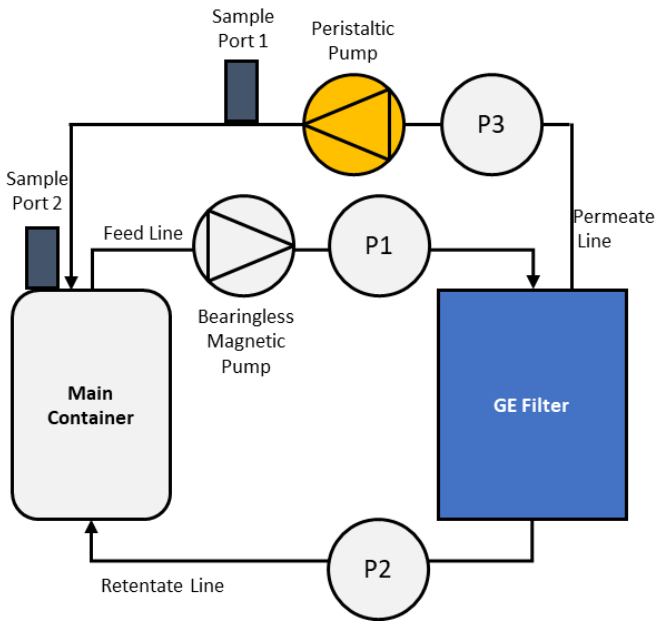

Figure 3-6. Filtration Set-up. *The schematic illustrates the filtration set-up used for all runs in the DOE. The feed solution (i.e., particle size fraction) was driven through the filter via a bearingless*

magnetic centrifugal pump. Particles smaller than the filter pore size permeated the filter, while particles greater than the filter pore size returned to the main container.

iii. Materials and Equipment

The **feed solution** was composed of the following materials. After combining the materials below, the feed solution was added to the main container.

- Particle Size Fraction – The primary component of the feed solution was supernatant (a.k.a. particle size fraction) – 75 mL of particle size fraction specified by the DOE was added to the main container. The volume of supernatant was determined via a series of loading experiments (**Appendix B**). The goal of the loading experiments was to determine the smallest loading (volume/filtration area) necessary to achieve known fouling profiles.
- Antibiotics – Because the supernatant is non-sterile, 0.75 mL of Penicillin-streptomycin was added to the main container prevent bacterial growth. The choice of antibiotics and determination of the dosage is discussed in **Appendix C**.
- Drug Substance (DS) – The DS used throughout the filtration runs were monoclonal immunoglobin antibodies (mAb IgG). DS was added to the main container to achieve 2 g of DS/L of supernatant, the concentration of DS typically used in Process Development experiments.

Two types of **pumps** were used across all runs: a centrifugal bearingless pump to drive the crossflow through the filter and a peristaltic pump to control the permeate flux.

- Centrifugal Bearingless Pump – Levitronix developed and manufactured the centrifugal bearingless pump (**Figure 3-7**). The pump head is composed of a motor and rotor magnet, which is completely encased in a chemical resistant, fluorocarbon material. The motor generates a

magnetic field that levitates and rotates the rotor magnet, which drives the fluid through the pump. Modulating the motor RPM controls the crossflow rate of fluid through the filter. Compared to peristaltic pumps, centrifugal bearingless pumps induce less hydrodynamic stress and lower rates of cell lysis [6]. Thus, the particles within each fraction are less likely to breakdown into smaller particles. Minimizing particle breakdown is important to maintain the distinct particle size fractions.

- Peristaltic Pump – The peristaltic pump was used to control permeate flux. We were less concerned about particle breakdown in the permeate line because we know that any particles that pass through the filter are smaller than the pore size. Thus, further breakdown of particles in the permeate would not impact the results.

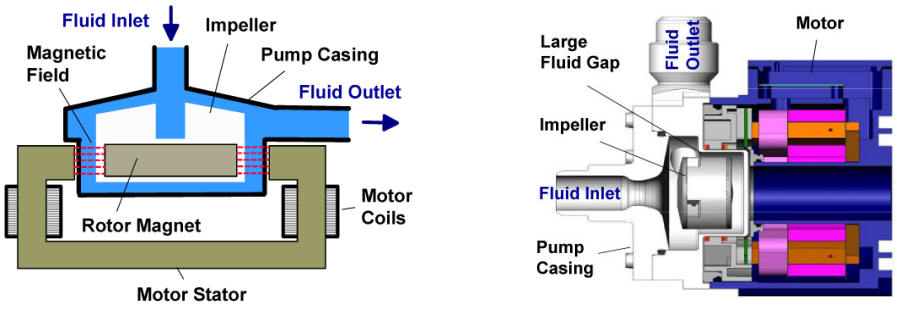

Figure 3-7. Levitronix Pump*. A bearingless magnetic centrifugal pump was used to drive crossflow through the filter* [38].

Microfiltration polysulfone cartridges of varying pore sizes were used across all runs. They were purchased in three pore sizes (750 kDa, 0.2 µm, and 0.45 µm) from GE Life Sciences (**Figure 3-8**). All filters encompassed a filtration area of 0.0038 m^2, the smallest filtration area available. A small filtration area was necessary to minimize the loading volume due to material constraints (see **Appendix B**). The dimensions of the filters were: Fiber Inner Diameter: 0.75 mm; Outer Diameter: 0.3 cm; Length: 60 cm;

Number of Fibers: 2; and Filtration Area: 0.0038 m^2. The filters, obtain from the same manufacturer, were single-use – one filter per filtration run – which is consistent with Amgen manufacturing practices.

Figure 3-8. Hollow Fiber Cartridge. *GE hollow fiber cartridges of varying pore sizes were used for all runs in the DOE.*

Single-use pressure sensors, manufactured by Pendotech, were connected to the cartridge inlet, outlet, and permeate end. The pressure sensors enabled the collection of pressure data and subsequent calculation of TMP. The readings were collected every ten seconds throughout all filtration runs and displayed in real-time by the Pendotech Data Acquisition System (DAQ).

In addition to the materials required for filtration, the **Cedex Bio HT Analyzer** was also utilized to measure the concentration (titer) of drug substance (DS) within the permeate and main container. The Cedex Bio HT, created by Roche, is a high-throughput, automated instrument that measures substrates, metabolites, and products (e.g., mAb) within cell culture. Two Cedex Bio HT assays were used to measure the titer within the permeate and main container samples: IGGHB and IGGHD. The primary difference between the assays is the detection range. IGGHB measures mAb concentration between 0.08 g/L and 8 g/L, while IGGHD measures IgG concentration between 0.4 g/L to 8 g/L. The initial concentration of IgG was 2 g/L, but with significant fouling the permeate concentration decreased to less than 0.4 g/L. Thus, though IGGHD was the primary assay, IGGHB was also necessary in cases of severe fouling.

Both assays measure titer using an antiserum (derived from rabbit) that contains a detection antibody against human IgG (**Figure 3-9**). The detection antibody binds to IgG within the sample, generating turbidity. The turbid solution (i.e., solution with antibody-antigen complexes) absorbs light at 340 nm, a different wavelength than the non-turbid solution. Thus, the amount of absorbed light with a wavelength of 340 nm is correlated with the concentration of IgG in the sample

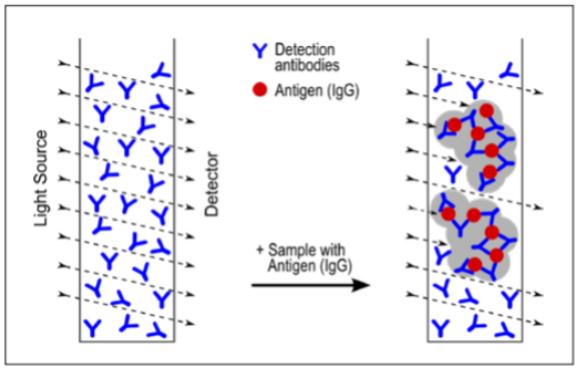

Figure 3-9. IgG Assay*. The Cedex Bio HT Analyzer measures the concentration of product using antiserum that contains a detection antibody against human IgG. The antibody-IgG complex absorbs wavelength at 340 nm, enabling the detection of IgG* [39].

iv. Detailed Protocol

The detailed protocol to conduct a single filtration run is outlined below. The protocol was replicated for all runs in the DOE.

1. The filter was flushed with ethanol (20%) and PBS. Flushing the filter is standard protocol to prime the filter and reduce initial fouling.

Flushing Solution	Crossflow	Permeate Line Open?	Stop Condition
Ethanol (20%)	20 mL/min	No	38 mL of retentate collected
Ethanol (20%)	20 mL/min	Yes	19 mL of permeate collected
PBS	20 mL/min	No	76 mL of retentate collected
PBS	20 mL/min	Yes	38 mL of permeate collected

Table 3-5. Filter Flush. *The filter was flushed with ethanol followed by PBS, both with and without the permeate line closed.*

2. The filtration system was set-up as illustrated in **Figure 3-6**. The pressure sensors were attached to the filter, and the tubing was thread through the crossflow and permeate pumps.
3. The feed solution was mixed together and added to the main container. The feed solution contained 75 mL of the particle size fraction specified in the DOE, 0.75 mL of antibiotics, and 2 mL of drug substance.
4. The Levitronix pump was primed by filling the pump head with 5 mL of feed solution (from the previous step).
5. The permeate line was closed and the crossflow was started by setting the Levitronix pumps to 3000 RPM (equivalent to 19.8 mL/min). The crossflow was run without permeate flux for twenty minutes – "crossflow only" time is standard protocol because it has been shown to minimize fouling.
6. After 20 minutes of "crossflow only" time, the flux was increased by 20% every 15 minutes until the desired final flux is reached. After the desired final flux was reached, the permeate flux and crossflow is maintained for 72 hours.

Time	Permeate Flux	Crossflow
0 – 20 minutes		19.8 ml/min
20 minutes	20% Final Flux	19.8 ml/min
35 minutes	40% Final Flux	19.8 ml/min
50 minutes	60% Final Flux	19.8 ml/min
65 minutes	80% Final Flux	19.8 ml/min
80 minutes	100% Final Flux	19.8 ml/min
80 minutes – 72 hours	100% Final Flux	19.8 ml/min

Table 3-6. Flux Ramp-up. *The permeate flux was ramped up every 15 minutes from 0% to 100% of the final flux.*

7. Immediately after the flux ramp-up (80 minutes), samples of the permeate and retentate were obtained through the sample ports (**Figure 3-6**). The titer in each sample was measured using the Cedex Bio HT and sieving was calculated by dividing permeate titer

by main container titer. This step was repeated at the following time points: 24 hours, 36 hours, 72 hours.

8. After 72 hours, the pressure data was exported and saved. The set-up was taken down and the steps 1-7 repeated for the next run.

D. Step 3: Polystyrene Microspheres Filtered using TFF

Polystyrene microspheres were also filtered using TFF, following the same protocol as Step 2 but with a different feed solution. In Step 2, the feed solution was comprised primarily of the particle size fraction specified in the DOE. In Step 3, the feed solution consisted of microspheres of a specific diameter, PBS, and drug substance. The purpose of filtering the microspheres was to elucidate the importance of particle size versus other particle size characteristics: e.g., chemistry and shape. If fouling was dependent on particle size, one would expect the microspheres and supernatant of similar diameters to exhibit the same sieving profiles. However, if microspheres exhibit no sieving decline, the data suggests that particle chemistry is as important or more important than particle size. The conditions compared are listed in **Table 3-7**. The concentration of microspheres in the microsphere solution was equivalent to the concentration of particles within the supernatant; the concentration of drug substance was also equivalent across the two solutions.

Pair Number	Supernatant Condition	Microsphere (MS) Condition
1	Particle Size: 0.65 – 1 µm Pore Size: 0.45 µm Permeate Flux: 9 LMH	MS Size: 1 µm Pore Size: 0.45 µm Permeate Flux: 9 LMH
2	Particle Size: < 0.1 µm Pore Size: 750 kDa Permeate Flux: 9 LMH	MS Size: 0.1 µm Pore Size: 750 kDa Permeate Flux: 9 LMH

Table 3-7. Microsphere Operating Conditions. *Microspheres were filtered under the same conditions as supernatant of the corresponding particle size. Microspheres served as a control – allowing the differentiation between particle size and chemistry.*

Chapter 4: Results and Discussion

The results are organized by the three experimental steps. **First,** the results of the supernatant fractionation and particle size analysis are presented: *Was the supernatant successfully separated into distinct particle size fractions?* **Second,** the results of the supernatant filtration data and analysis are presented: *Which factors are correlated with fouling, as measured by low sieving and high TMP?* **Finally,** the microsphere filtration data and analysis are presented: *Is particle size truly impacting fouling?*

A. Step 1: Results of Fractionation

The particle size distribution of each fraction, measured using Dynamic Light Scattering (DLS), are summarized in **Table 4-1**. The results demonstrate that for most particle size fractions, the average peak particle diameter fell within the expected range – i.e., the range of filter pore sizes used to generate the particle size fraction. For the two smallest particle size fractions, Fraction <0.1 μm and Fraction 0.1-0.22 μm, the average peak particle diameter was slightly higher than the expected range. The higher than expected diameter suggests slight particle aggregation. Even with slight aggregation, Fraction <0.1 and Fraction 0.1-0.22 μm still contained the smallest and second smallest particles. Thus, the discrepancy between the theorized and measured results was not of concern.

The standard deviation of the DLS readings was substantial for the larger particle size fractions, most notably Fraction 0.45-0.65 μm and Fraction 0.65-5 μm. For Fraction 0.65-5 μm, a large standard deviation was expected for two reasons: 1) the range of pore sizes was expected to be several microns;

2) DLS does not precisely measure particles greater than several microns. For Fraction 0.45-0.65 µm, a large standard deviation was unexpected. A potential reason for the large standard deviation is that the particles within this fraction may have non-spherical shapes. Non-spherical shapes would result in widely different measurements depending on which side diffracts the incident light because DLS assumes spherical particles.

Overall, the data demonstrate that the particle size fractions were fairly distinct. The average peak particle diameter increased as expected – e.g., Fraction 1 contained the smallest particles, and Fraction 6 contained the largest particles. Moreover, the percent mass within the peak is over 95%, meaning the majority of the particles fell within the measured range. The proximity of the median and the mean also suggests a discrete peak (as opposed to long tails). For these reasons, the fractionation was deemed sufficient to discern the effects of different particle size bands, and the average peak particle size was utilized for the remainder of the analysis.

Fraction	Theorized Particle Diameter	# of Readings	Median Particle Diameter (µm)	Avg. Peak Particle Diameter (µm) Mean +/- Std. Dev.	Avg. % Mass in Peak
Fraction 1	<0.1 µm	219	175.690	0.174 +/- 0.033	>98%
Fraction 2	0.1 – 0.22 µm	82	215.000	0.285 +/- 0.191	>98%
Fraction 3	0.22 – 0.45 µm	159	337.959	0.342 +/- 0.082	>98%
Fraction 4	0.45 – 0.65 µm	116	466.642	0.578 +/- 0.598	>95%
Fraction 5	0.65 – 1 µm	97	800.60	0.732 +/- 0.187	>98%
Fraction 6	0.65 – 5 µm	46	1486.9470	1.511 +/- 0.632	>98%

Table 4-1. Dynamic Light Scattering (DLS) Results. *The table displays the results from measuring the particle size using DLS. DLS measured the mean diameter of particles within the sample.*

B. Step 2: Results of Filtration of Supernatant Fractions

The two dependent variables that were measured throughout each run were: transmembrane pressure and sieving. Both transmembrane (TMP) and sieving are indicators of fouling and thus were used to assess the degree of fouling during each run. The relationship between the operating conditions (particle size, pore size, permeate flux) and the degree of fouling was determined using linear regression. Finally, sieving was translated into an estimate of harvest yield to evaluate the productivity losses under the varying operating conditions.

i. Overview of Response Variables

Transmembrane Pressure: TMP is equal to the average of the inlet and outlet pressures less the permeate pressure (**Eq. 4-1**):

$$TMP = \frac{(P_{in} + P_{out})}{2} - P_{perm}$$

As reviewed in **Chapter 3**, the Pendotech Pressure System recorded P_{in}, P_{out}, and P_{perm}, measured every ten seconds for three days (25,920 data points). The raw data was converted to TMP using the formula above. The converted data indicated that the majority of conditions (17 of 40 runs) exhibited minimal pressure increases over the three-day experiment, which suggests no to minimal fouling. 8 of 40 conditions exhibited sharp increases in TMP within the first few hours of the run, suggesting rapid fouling. The remaining conditions exhibited steady increases in TMP (15 of 40 runs). An example of each condition – no, moderate, and rapid TMP increase – is displayed in **Figure 4-1**.

Because the permeate pump rotated at a constant RPM (Peristaltic Pump in **Figure 3-6**), the flux was assumed to remain constant while the TMP was increasing. From Darcy's Law (**Eq. 4-2)**:

$$J = \frac{TMP}{\mu(R_M + R_R + R_I)}$$

, if flux is constant, TMP increases to compensate for increased membrane resistance from fouling. However, the TMP eventually reached a maximum value of 18 psi due to inefficiencies in the peristaltic pump. Beyond the maximum TMP, the pressure stabilized, and the flux decreased with increased membrane resistance according to Darcy's Law (**Eq. 4-2**). Thus, for the eight conditions that reached a steady-state TMP within the first hour of the run, the flux decreased significantly to compensate for additional membrane resistance (e.g., Run 11 in **Figure 4-1**). In contrast, for the 15 conditions that exhibited gradual increases in TMP, the flux is assumed to remain constant until the maximal pressure is reached (e.g., Run 30 in **Figure 4-1**).

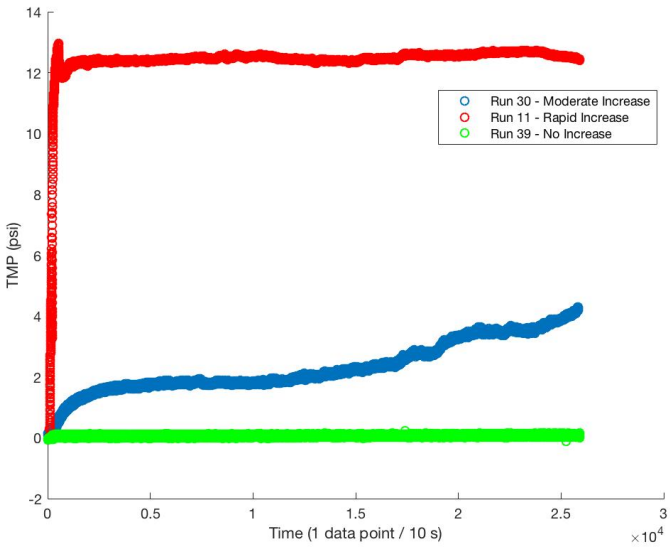

Figure 4-1. TMP Categorization. *The figure displays three TMP curves. Run 39 exhibited no TMP increase over the course of the experiment, while Run 11 exhibited a rapid TMP increase. Run 30 only exhibited a moderate increase in TMP over the course of the experiment.*

Before conducting the regression analysis, the average TMP was calculated for each run (**Eq. 4-3**):

$$TMP_{avg} = \sum_{0}^{T} \frac{TMP_T}{T}$$

The higher the TMP, the greater the extent of fouling. For scale, the maximum pressure tolerated by the system was 18 psi – at 18 psi, the pressure stabilized, and the flux decreased with increased membrane resistance according to Darcy's Law. Thus, the maximum TMP_{avg} was 18 psi, which only was met if the maximum pressure was maintained throughout the entire run. The minimum TMP_{avg} was 0 psi because the permeate pressure was less than the average of the inlet and outlet pressure by design. The average TMP across all runs was 3.95 psi with a standard deviation of +/- 4.41 psi. Given the large standard deviation relative to the average, there was immense variability in TMP across the various operating conditions.

Sieving: As the membrane fouls, sieving (i.e., product passage) typically decreases. Thus, sieving is not only an indicator of fouling but also a proxy for overall product yield. Sieving was calculated for every run at hours 0, 24, 48, and 72. To calculate sieving, the concentration of product in the permeate was divided by the concentration of product in the retentate (**Eq. 4-4**). If there is no fouling, sieving is close to 100% because the product can readily permeate the membrane. As the membrane fouls, the product cannot readily permeate the membrane and sieving decreases.

$$Sieving = 100\% \times \frac{Permeate\ Concentration}{Retenate\ Concentration}$$

Like with TMP, the average sieving was calculated for each run. The feasible range of average sieving values were between 0% to 100%, where the former represents no product passage while the later represents complete passage. The mean of the average sieving values across all runs was 67.80% with a standard deviation of +/- 26.13%.

Harvest: The sieving data was converted to harvest yield – the metric that ultimately impacts the bottom-line. The following schematic illustrates how the sieving data was converted to harvest yield.

The permeate concentration is a product of the retentate initial concentration and sieving. The amount of product that permeates the filter is then subtracted from the retentate to calculate the final retentate concentration. The overall harvest yield is the final permeate concentration over the initial retentate concentration, e.g., 4/6 x 100% = 66.67% in **Figure 4-2**. Across all runs, the average harvest yield was 66.69% +/- 21.82%.

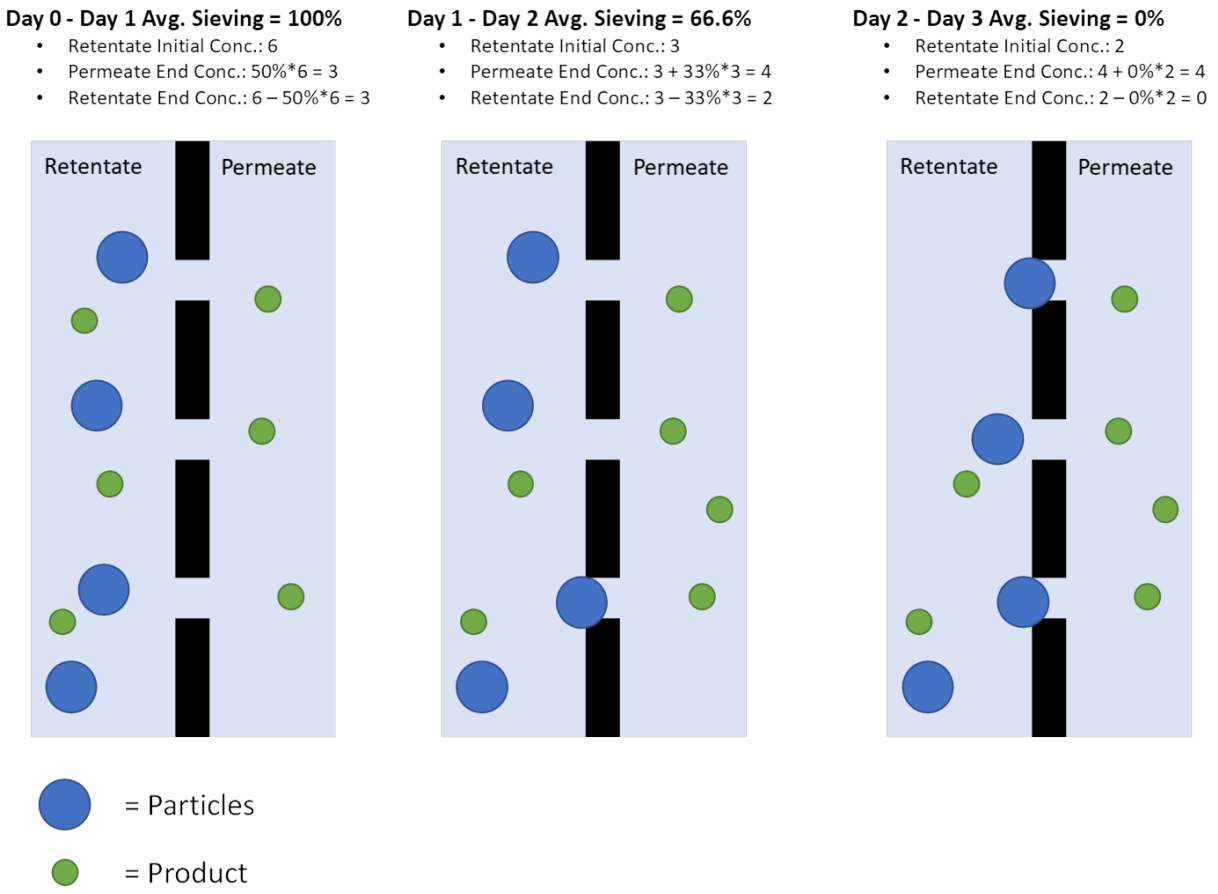

Figure 4-2. Harvest Calculation. *The schematic illustrates the conversion of sieving data to harvest yield.*

ii. Main Effect Plots

Main effect plots plot the mean response at each level of the independent variables. The main effect plots of the response variables – TMP, sieving, and harvest yield – display similar trends (**Figure 4-3**).

First, the results illustrate that there is not a linear relationship between particle size and the response variables – a linear fit gives an adjusted R^2 of less than 0.1. However, the <0.1 μm fraction appears to be an outlier, and the primary reason for the poor linear fit. Removing the <0.1 μm fraction increases the adjusted R^2 to across all response variables to greater than 0.8, suggesting a linear relationship between particle size and TMP, sieving, and harvest yield for the majority of particle sizes. There also appears to be a strong linear relationship between flux and the response variables, with an R^2 of greater than 0.95. In contrast, there appears to be no relationship between pore size and the response variables.

Importantly, the correlation direction for each independent variable is consistent across the response variables. The purpose of measuring TMP, sieving, and harvest yield is that all three variables are indicators of fouling. If increasing an independent variable causes fouling, TMP is expected to increase, while sieving and harvest yield are expected to decrease. The reverse is also true: if increasing an independent variable decreases fouling, the TMP is expected to decrease while sieving and harvest yield are expected to increase. Thus, the main effect plots illustrate the following:

- With the exception of the <0.1 μm fraction, particle size is positively correlated with fouling (increasing the particle size is associated with increases TMP and decreases sieving/harvest yield).
- Flux is negatively correlated with fouling (decreasing the flux is associated with decreases TMP and increases sieving/harvest yield).
- Pore size is not correlated with fouling.

Of note, the standard deviation of the response variables varies widely by particle size. For example, the standard deviation of the average TMP for runs with particles <0.1 μm is 3.84 psi, suggesting that runs

within one standard deviation of the mean exhibit varying degrees of fouling. In contrast, the standard deviation of the average TMP for runs with particles between 0.1-0.22 μm is 0.42 psi, one-tenth of the standard deviation of the <0.1 μm fraction. The differences in standard deviation suggest that the level of fouling (as measured by average TMP) is dictated by different factors in each particle size group. The narrow range of responses for the 0.1-0.22 μm fraction suggests that for this fraction, particle size primarily drives the extent of fouling. That is, there is minimal fouling across all runs with 0.1-0.22 μm particles, no matter the pore size or flux. The large standard deviations of the remaining particle size fractions suggest that for these fractions, particle size alone does not dictate the extent of fouling – pore size and/or flux likely also influence fouling.

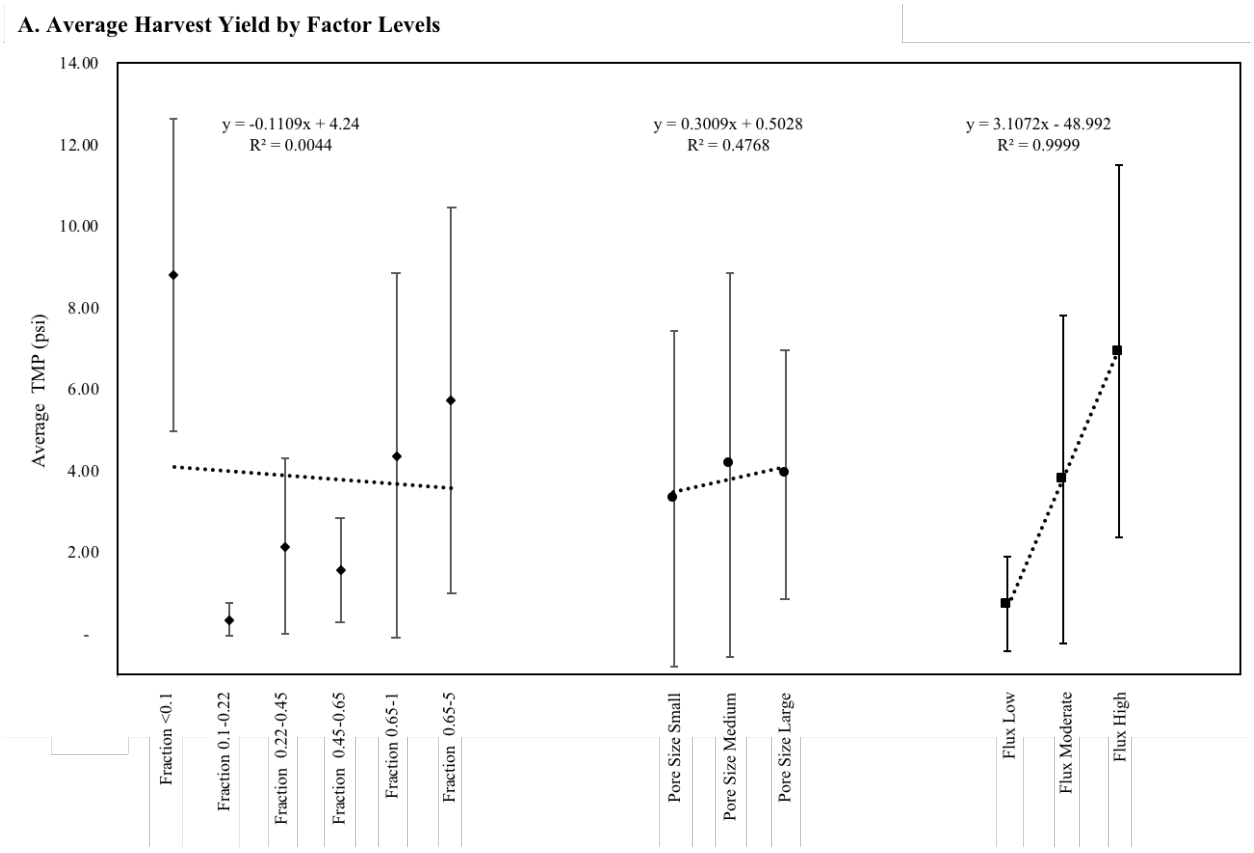

B. Average Harvest Yield by Factor Levels (without Fraction <0.1 um)

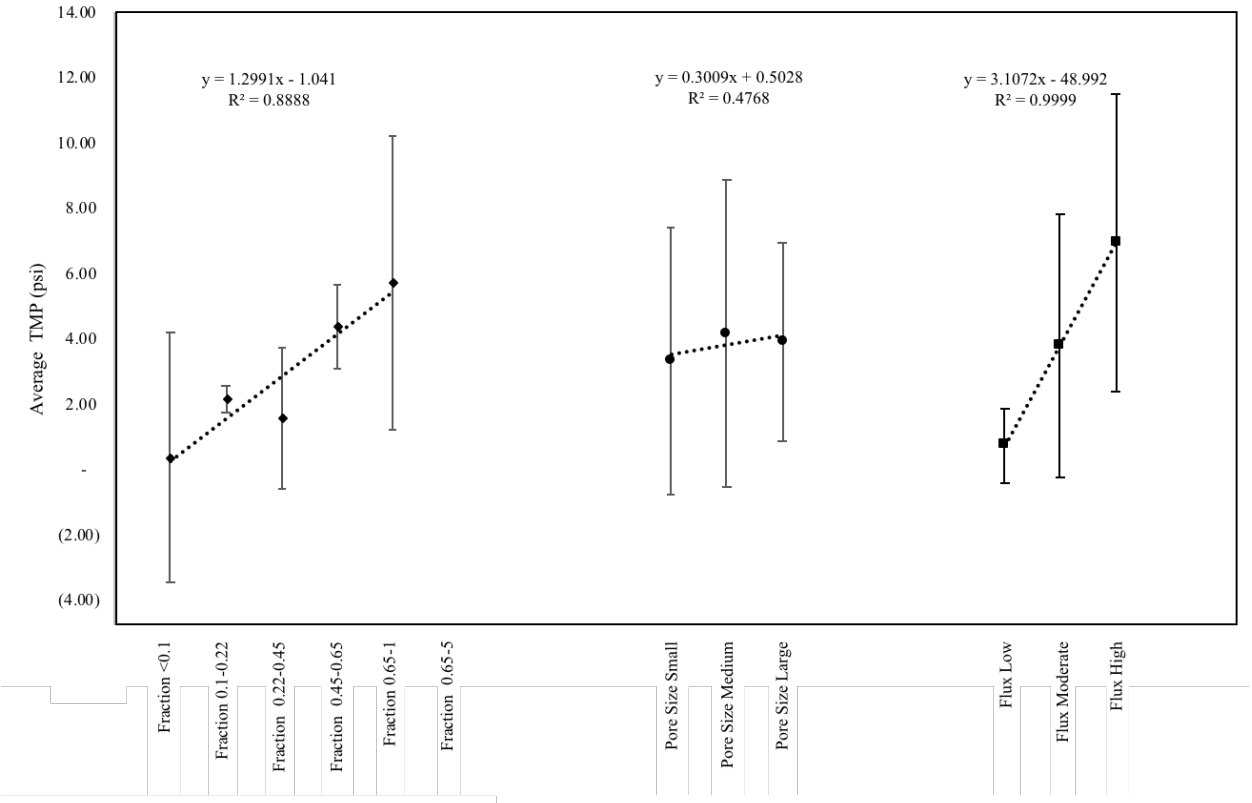

C. Average Sieving by Factor Levels

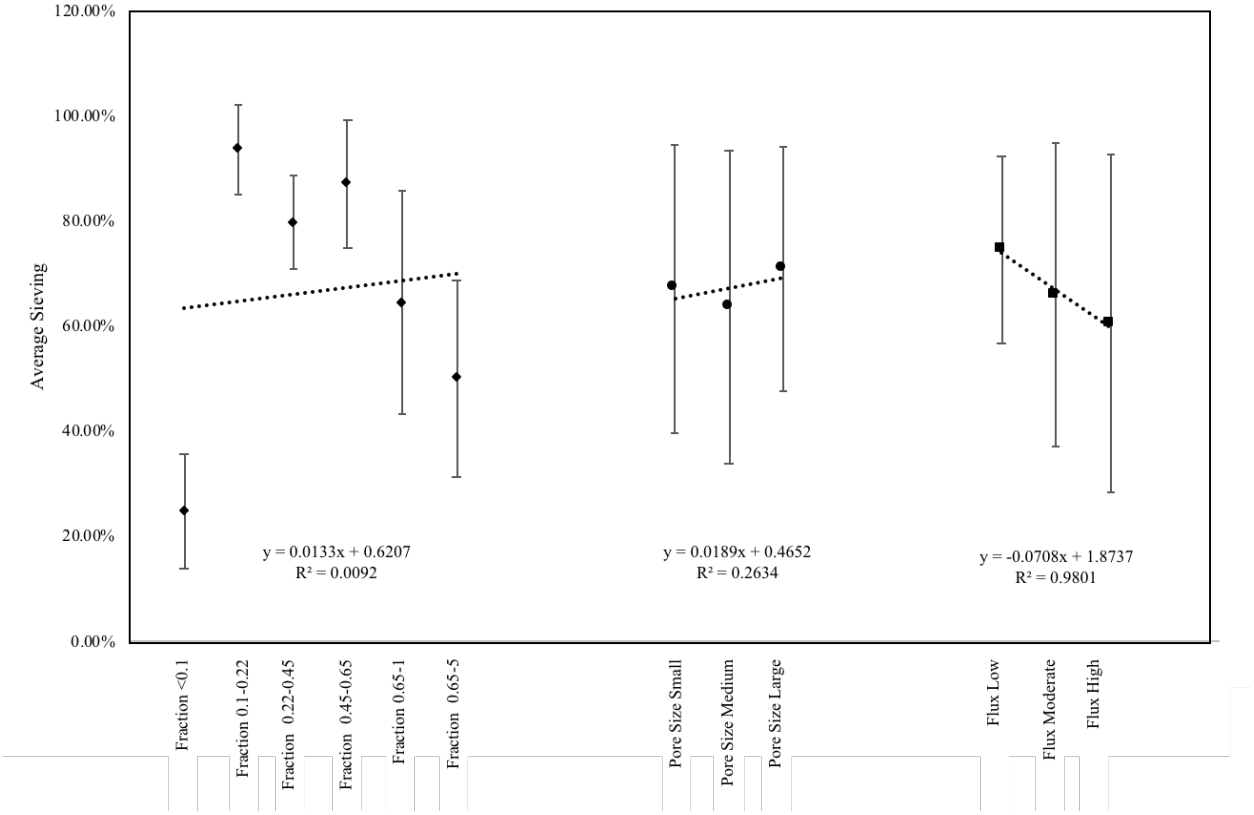

D. Average Sieving by Factor Levels (without Fraction <0.1 um)

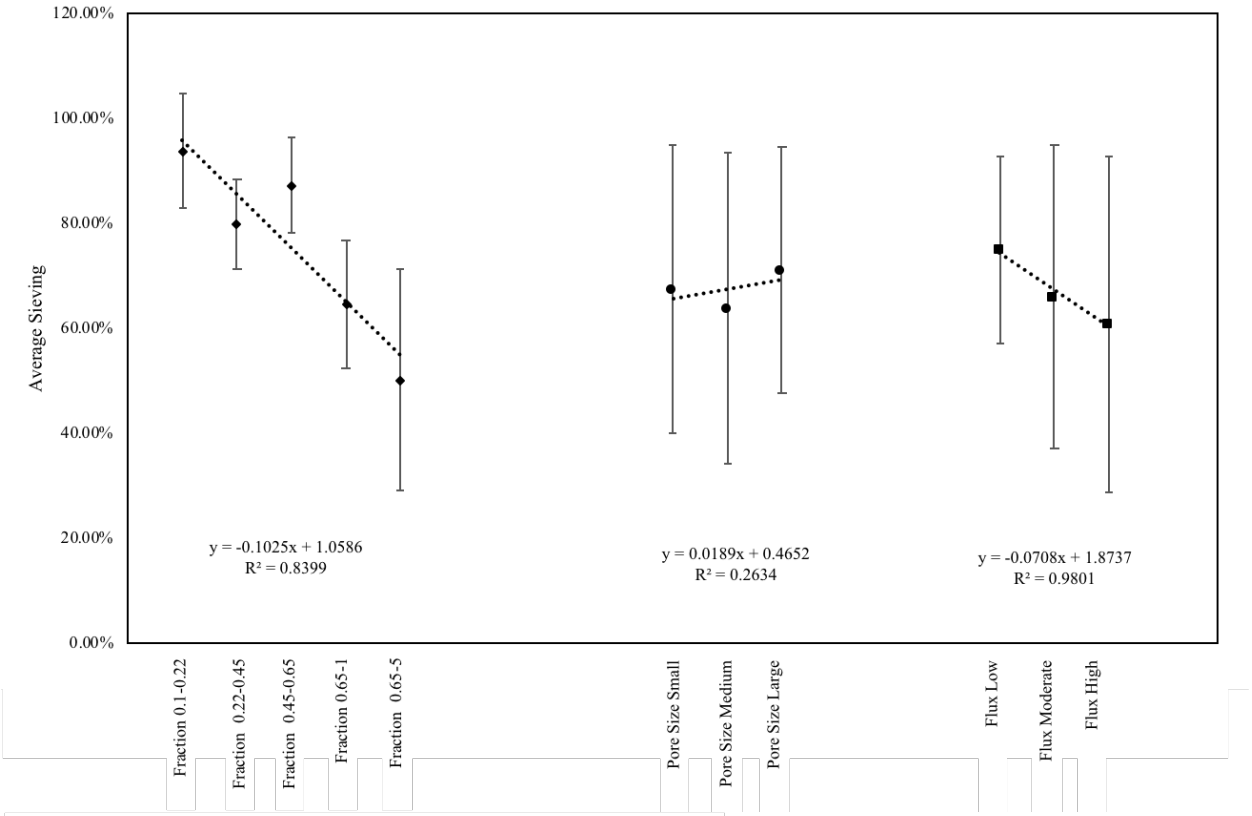

E. Average Harvest Yield by Factor Levels

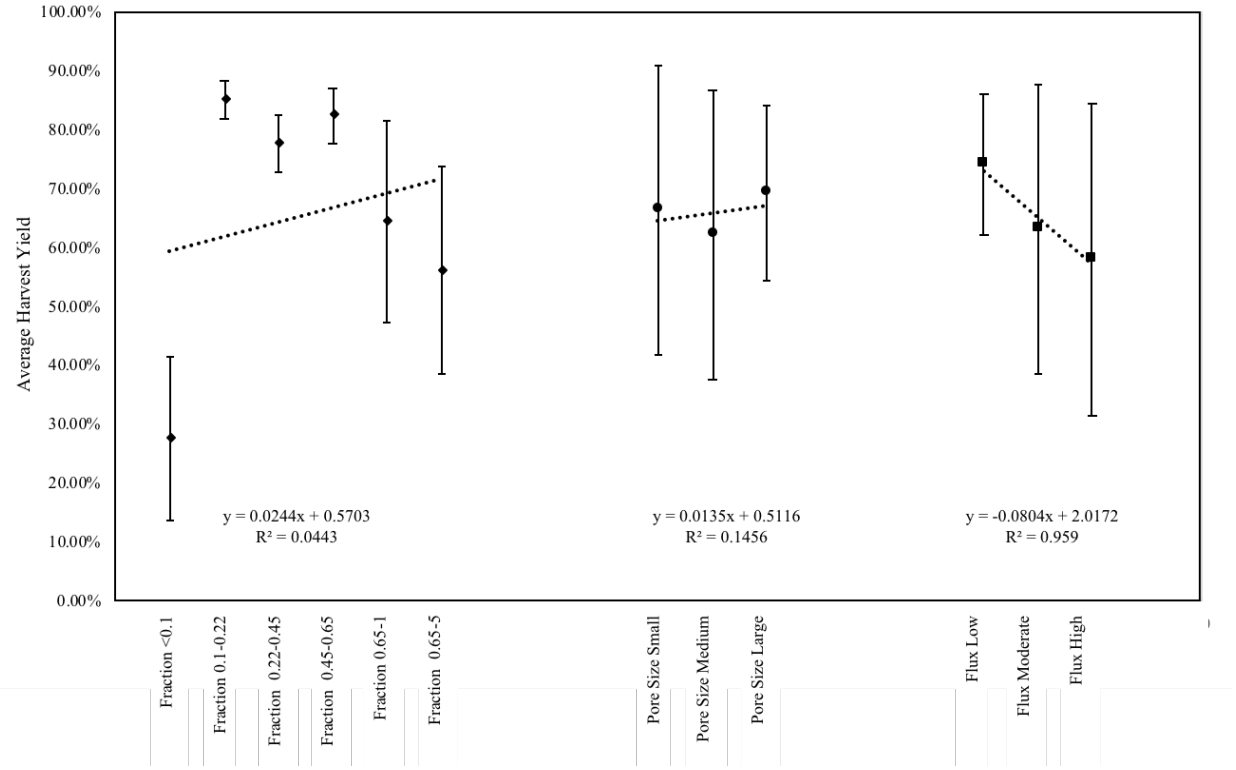

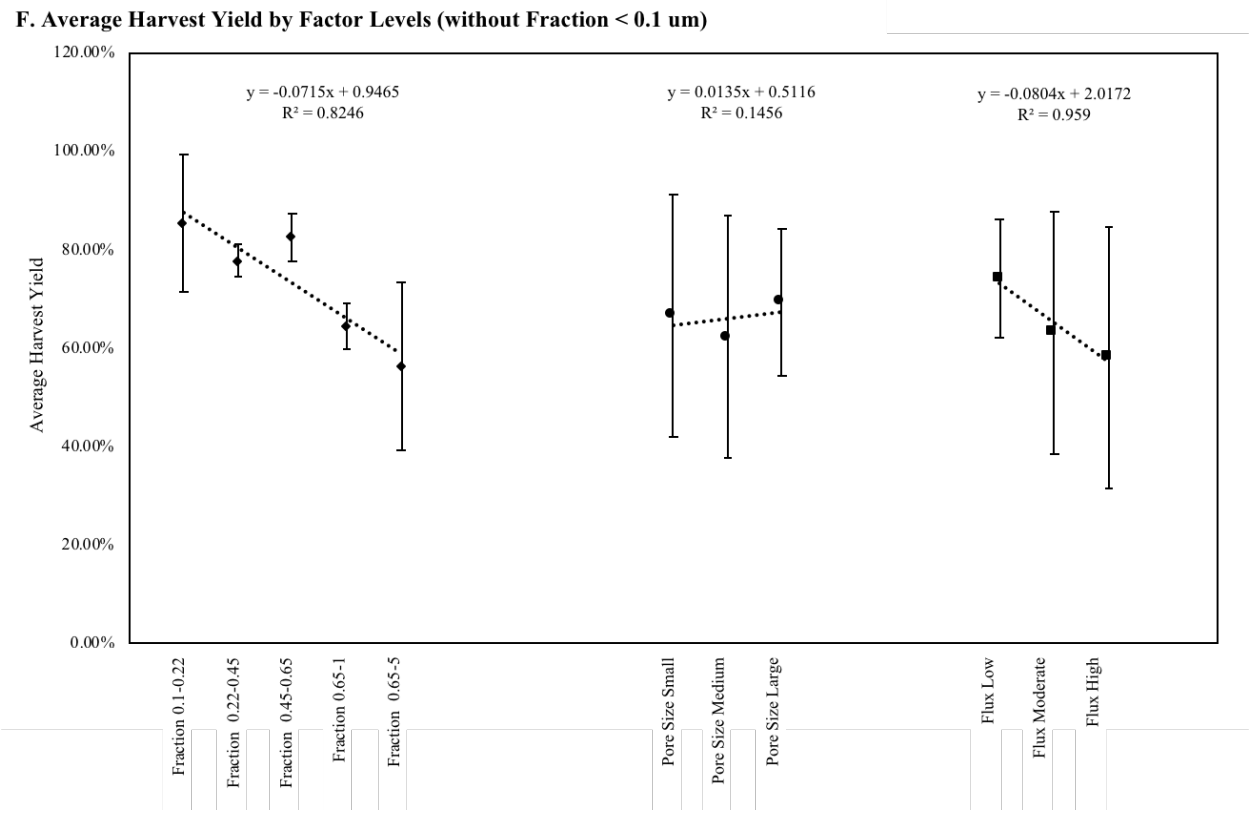

Figure 4-3. Main Effect Plots. *A) The average TMP is plotted for all levels of each independent variable. E.g., the average TMP is plotted for all runs using Fraction <0.1 µm, all runs using Fraction 0.1-0.22 µm, and etc. B) The average TMP is plotted for all levels after removing Fraction <0.1 µm. C). The average sieving is plotted for all levels of each independent variable. D) The average sieving is plotted for all levels after removing Fraction <0.1 µm E). The average harvest yield is plotted for all levels of each independent variable. F) The average harvest yield is plotted for all levels after removing Fraction <0.1 µm*

iii. Model Analysis

The independent variables were fit to the following models (**Eq. 4-5, Eq. 4-6, Eq. 4-7**) to assess their relationship with the corresponding response variables. Note that the DOE was designed assuming the same models.

$$A \cdot Pore\ Size + B \cdot Flux + C \cdot Particle\ Size + D \cdot Pore\ Size \cdot Flux + E \cdot Pore\ Size \cdot Particle\ Size + F \cdot Flux \cdot Particle\ Size + G = Avg\ TMP$$

$$A \cdot Pore\ Size + B \cdot Flux + C \cdot Particle\ Size + D \cdot Pore\ Size \cdot Flux + E \cdot Pore\ Size \cdot Particle\ Size + F \cdot Flux \cdot Particle\ Size + G = Avg\ Sieving$$

$$A \cdot Pore\ Size + B \cdot Flux + C \cdot Particle\ Size + D \cdot Pore\ Size \cdot Flux + E \cdot Pore\ Size \cdot Particle\ Size + F \cdot Flux \cdot Particle\ Size + G = Harvest\ Yield$$

The models poorly fit the data, as indicated by the low adjusted R^2 values (**Table 4-2**). Moreover, the F-ratios for the models of average sieving and harvest yield were not statistically significant, meaning that the models did not improve fit compared to taking the average for all values (**Table 4-2**). In addition to the variables within **Eq. 4-5 to Eq. 4-7**, the following variables were also a potential source of variation and were iteratively incorporated into the model: pump number, filter batch number, and run number. However, none were evaluated to be statistically significant (**Appendix D**).

	TMP		Sieving		Harvest	
Summary of Fit	**Value**	**p-value**	**Value**	**p-value**	**Value**	**p-value**
R-square Adj	0.2864	N/A	-0.0537	N/A	-0.0320	N/A
F-ratio	**3.7419**	**0.0056***	0.6516	0.6885	0.7882	0.5852
Parameter	**Value**	**p-value**	**Value**	**p-value**	**Value**	**p-value**
Intercept (psi)	-1.9336	0.2882	**0.7701**	**<0.0001***	**0.7511**	**<0.0001***
Pore Size (psi/µm)	-0.4454	0.9135	0.1877	0.5503	0.1622	0.5374
Flux (psi/LMH)	**0.5721**	**0.0002***	-0.0126	0.2296	-0.0143	0.1065
Particle Size (psi/µm)	0.6711	0.5852	-0.0380	0.6862	0.0072	0.9270
Pore Size*Flux (psi/µm/LMH)	0.3142	0.7389	-0.1697	0.8013	0.0076	0.8996
Particle Size*Pore Size (psi/ μm^2)	-1.001	0.9096	-0.0187	0.7949	-0.0756	0.8934
Flux*Particle Size (psi/µm/LMH)	0.4491	0.1177	-0.0256	0.2399	-0.0217	0.2345

Table 4-2. Model Results (with Fraction <0.1 µm). *The table shows the results of fitting the empirical data to the following model:* A·Pore Size + B·Flux + C·Particle Size + D·Pore Size·Flux + E·Pore Size·Particle Size + F·Flux·Particle Size + G = Response Variable*. The bolded coefficients and starred p-values are statistically significant at an alpha of <0.05. The model fit the data poorly as exemplified by the lack of statistical significance.*

The models above assume that the primary interaction between the independent variable and the response variable is linear. For example, the term *"... C*Particle Size... = Avg TMP"* forces a linear relationship between Particle Size and Average TMP. However, as displayed in the main effect plots, there does not appear to be a linear relationship between particle size and the response variable if all

particle sizes are included. If the <0.1 μm particle size fraction is removed, though, the relationship is linear. Thus, the same models were re-evaluated with the <0.1 μm particle size fraction excluded. Biologically, the existence of an outlier suggests that the particles within the <0.1 μm particle size fraction are interacting with the membrane and/or each other differently than the other particles. For example, <0.1 particles may be more hydrophobic than the other particles and thus aggregate at the surface of the hydrophobic polysulfone membrane [40]. Fraction <0.1 μm is further discussed in **Section 6 and 7** below.

The model fit drastically improved after removing the <0.1 μm particle size fraction (**Table 4-3**). For all response variables, the model was statistically significant (F-ratio p-value <0.05).

	TMP		Sieving		Harvest	
Summary of Fit	**Value**	**p-value**	**Value**	**p-value**	**Value**	**p-value**
R-square Adj	0.6829	N/A	0.4725	N/A	0.5137	N/A
F-ratio	**13.5615**	**<0.0001***	**6.2257**	**0.0003***	**7.1612**	**<0.0001***
Parameter	**Value**	**p-value**	**Value**	**p-value**	**Value**	**p-value**
Intercept (psi)	**-4.8186**	**0.0002***	**1.0265**	**<0.0001***	**0.9631**	**<0.0001***
Pore Size (psi/μm)	1.0320	0.6836	0.0880	0.6397	0.0534	0.6981
Flux (psi/LMH)	**0.5484**	**<0.0001***	-0.0114	0.0733	**-0.0120**	**0.0112***
Particle Size (psi/μm)	**3.0232**	**0.0003***	**-0.2631**	**<0.0001***	**-0.1831**	**<0.0001***
Pore Size*Flux (psi/μm/LMH)	-0.4746	0.5300	-0.0486	0.2733	-0.0094	0.7682
Particle Size*Pore Size (psi/ μm^2)	-3.4497	0.5300	-0.0597	0.8841	0.1141	0.6983
Flux*Particle Size (psi/μm/LMH)	**0.5951**	**0.0020***	**-0.0292**	**0.0322***	**-0.0284**	**0.0053***

Table 4-3. Model Results (without Fraction <0.1 μm). *The table shows the results of fitting the empirical data (excluding Fraction <0.1 μm) to the following model:* A·Pore Size + B·Flux + C·Particle Size + D·Pore Size·Flux + E·Pore Size·Particle Size + F·Flux·Particle Size + G = Response Variable. *The bolded coefficients and starred p-values are statistically significant at an alpha of <0.05. The model fit improved significantly after excluding Fraction <0.1 μm.*

Particle size is statistically significant across all response variables. Increasing the particle size by 1 μm increases fouling, as indicated by an increase in TMP (3.02 psi/1 μm), a decrease in sieving (-26.31%/1 μm), and a decrease in overall harvest yield (-18.31%). **Permeate flux** is also statistically significant for TMP and harvest yield. Like particle size, increasing flux by 1 LMH increases the extent of fouling – increasing flux by 1 LMH is associated with a 0.55 psi increase in TMP and a 1.20% decrease in harvest yield. The positive relationship between flux and fouling aligns with both mechanistic models and previous studies. Mechanistically, permeate flux increases the force driving particles toward the membrane surface, leading to greater fouling. Moreover, a positive relationship between permeate flux and fouling has been demonstrated repeatedly in literature [8][5].

Though the coefficients on particle size are larger in magnitude than those on flux, the range of particle sizes was narrower than that of fluxes. Thus, the effect sizes of particle size and flux are approximately equal after weighting the coefficients by the feasible range: e.g., (-18.31%/1 μm)*~1 μm = 18.31% change in harvest yield over the complete range of particle sizes; (-1.20%/1 LMH)*~10.5 LMH = 12.6% change in harvest yield over the complete range of fluxes.

Overall, particle size and flux have a greater effect on TMP than on sieving and harvest yield because TMP is a direct consequence of fouling while sieving and harvest yield are indirect consequences of fouling. According to Darcy's Law, an increase in membrane resistance causes an increase in TMP and/or decrease in permeate flux (**Eq. 4-8)**:

$$J = \frac{TMP}{\mu(R_M+R_R+R_I)}.$$

In contrast, sieving and harvest yield may remain high even as the membrane fouls if the permeate flux holds constant. The permeate flux remains constant until TMP reaches its maximal value. After TMP

stabilizes, the permeate flux decreases with increased resistance, and sieving and harvest yield decrease. Sieving and harvest yield may also decline while permeate flux is constant if the filter pore size decreases due to standard blocking.

The **interaction between particle size and flux** was also statistically significant across all response variables. As the pore size and/or flux increase, the magnitude of their effect on the response variables increases. For illustration, compare two conditions: one with a pore size of 1 μm and a flux of 10 LMH, and the second with a pore size of 0.5 μm and a flux of 5 LMH. The average TMP is approximately the sum of the main effect of flux, the main effect of particle size, and the flux-particle size interaction:

$$Case\ 1: \quad 0.55\frac{psi}{LMH} \cdot 10\ LMH + 3.02\frac{psi}{\mu m} \cdot 1\ \mu m + 0.60\frac{psi}{LMH \cdot \mu m} \cdot 10\ LMH \cdot 1\ \mu m = 14.52\ \text{psi}$$

$$Case\ 2: \quad 0.55\frac{psi}{LMH} \cdot 5\ LMH + 3.02\frac{psi}{\mu m} \cdot 0.5\ \mu m + 0.60\frac{psi}{LMH \cdot \mu m} \cdot 5\ LMH \cdot 0.5\ \mu m = 5.76\ \text{psi}$$

Though flux and particle size are simply doubled from Case 2 to Case 1, the TMP in Case 1 is ~2.5X that of Case 2. The amplification effect is due to the interaction between particle size and flux: as the particle size increases, the effect of flux on fouling increases (and vice versa). The interaction effect is best understood through Stoke's Law, which derives the drag force on a small sphere through viscous fluid (**Eq. 4-9)**:

$$F_D = 6\pi\mu R v \Omega$$

, where Ω is Happel's correction factor for crossflow) [41]. The drag forces on the particles within the filter can be decomposed into an x- and y-direction, the former due to crossflow and the later due to permeate flow. In the y-direction, the drag forces point toward the membrane surface and are dependent on R – the radius of the particle – and v – the permeate flow rate. Thus, increasing either the size of the particle or the permeate flux increases the driving force toward the membrane surface and thus the extent of fouling.

The **pore size, and any interaction term involving pore size**, is not statistically significant across the response variables. Changing the pore size does not significantly impact the extent of fouling, as measured by TMP, sieving, and harvest yield. If only particle size was important (and not chemistry or shape), one would expect a "critical ratio" of particle size to pore size above which fouling occurs and below which fouling does not occur. However, there does not appear to be a critical ratio because the particle size main effect is unaffected by filter pore size. Thus, caking is primarily occurring – unlike other methods of fouling, caking is independent of pore size. Caking is expected because for the majority of the conditions studied, the particle size is at least as large as the pore size.

iv. Evaluation of Hypothesis

Based on the model results (**Table 4-3**), our hypothesis was evaluated. We hypothesized that: 1) the degree of fouling is dependent on particle size, and 2) for a given particle size fraction, the extent of fouling is impacted by pore size and/or flux.

- The main effect of particle size supports our hypothesis that the degree of fouling is dependent on particle size. Increasing the particle size is associated with increased fouling and decreased harvest yield (18.31% decreased in harvest yield per 1 μm increase in particle size).
- The interaction term between particle size and permeate flux supports our hypothesis that for a given particle size fraction, the extent of fouling is impacted by flux. The model suggests that the main effect of flux and particle size are amplified as either independent variable is increased.
- The lack of significance of the interaction term between particle size and pore size refutes our hypothesis that for a given particle size fraction, the extent of fouling is impacted by the filter

pore size. The model suggests that 1) particle size and pore size are independent, and 2) pore size and fouling are independent.

v. Business Implications

Of the three response variables, harvest yield is not only the most tangible but also has the greatest implications for business decisions. The results demonstrated that large particles are associated with decreases in harvest yield: particles ~ 1 μm are associated with a 18.31% decrease in harvest yield, seemingly because of their size. Such large decreases in harvest yield represent a significant loss of productivity and increase in costs. Thus, large cell debris should be eliminated to increase the robustness and reliability of harvest. Possible methods to remove the cell debris include:

- Switching to pumps that induce less shear (e.g., bearingless centrifugal pump) to reduce the formation of cell debris
- Utilizing cell-line engineering techniques to genetically alter anti-apoptotic genes to maintain higher cell viability
- Shifting the start of harvest earlier by reducing the duration of the production bioreactor step, thereby harvesting the product before the cell viability decreases

These potential solutions and their capacity implications are explored below.

<u>Case Study: Switching to Lower Shear Pumps</u>

Several pumps induce lower hydrodynamic stress compared to peristaltic pumps, which are typically used in TFF-based microfiltration. For example, the centrifugal bearingless pumps used throughout

this experiment induce less hydrodynamic stress and have lower rates of cell lysis [6]. The pump head is composed of a motor and rotor magnet, which is completely encased in a chemical resistant, fluorocarbon material. The motor generates a magnetic field that levitates and rotates the rotor magnet, which drives the fluid through the pump. Modulating the motor RPM controls the crossflow rate of fluid through the filter.

Based on the results, a decrease in cell debris, most notably larger cell debris, will increase the overall harvest yield and thus production capacity. From the model (**Table 4-3**), ~ 1 µm cell debris at a concentration typically seen with perfusion processes is associated with a -18.31% decrease in harvest yield. Thus, eliminating the majority of ~1 µm cell debris could increase harvest yield and thus capacity by 18.31%. Though completely eliminating all large cell debris is likely infeasible, any reduction in concentration will likely improve yield. Assuming a linear dependency between the concentration of ~ 1 µm cell debris and harvest yield, decreasing the concentration of large cell debris by half will increase yield and capacity by ~9%.

Alternatively, ATF/TFF-microfiltration could be replaced with novel technologies that are not associated with fouling. For example, acoustic wave separators are being explored to harvest product from high-density cell culture. Acoustic forces generate waves across a flow channel. As the cell culture flows through the channel, the cells are "trapped" by the waves while the product and smaller particles can permeate the acoustic waves into an outlet channel [17]. Because the acoustic wave separator does not rely on filters, fouling is not a problem. However, the scale-up of acoustic wave separators remains a challenge [17].

Case Study: Engineering Cells to Alter Anti-Apoptotic Genes

Cell death pathways include apoptosis and necrosis. Apoptosis is programmed cell death – it is a physiological process by which unwanted or useless cells are eliminated during the development and other normal biological processes. In contrast, necrosis is a pathological process that occurs when cells are exposed to external triggers. In harvest, apoptotic triggers are dependent on bioreactor and ATF/TFF design. Media lot hold time and feed strategy affect nutrient availability, and ATF hold-up and poor mixing cause oxygen depletion.

Engineering cells to alter anti-apoptotic genes is a promising strategy to minimize cell-death and thus debris that causes fouling. Previous work has demonstrated that engineering CHO cells to overexpress anti-apoptotic genes (Bcl-2, Bc1-x, and Mcl-1) or suppress apoptotic genes (Bak and Bax) decreased cell death [42]. Consequently, there would be a lower concentration of cell debris, leading to less fouling and higher harvest yield. An additional benefit of this strategy is that the bioreactor titer may also increase. Because more cells are alive, more cells are produing the therapeutic product, leading to higher titers. The increased protein production after altering genes related to the apoptosis pathway has been demonstrated empirically [42]. The dual benefits – decreased cell debris and increased titer – would undoubtedly increase overall capacity.

Case Study: Shifting Harvest Yield

The final option not only increases harvest yield through the reduction of cell debris but also through increased bioreactor turnover. As illustrated in **Figure 4-4**, titer in the production bioreactor continues to increase after cell viability has decreased. Thus, there is a tradeoff between maximizing titer and

decreasing cell debris. To simplify the calculations, assume that at max titer (*Time* = *T*) there is significant ~ 1 µm cell debris while at max density (*Time* = *T-x*) there is minimal ~1 µm cell debris. The trade-off calculation reduces to (**Eq. 4-10**):

$$\frac{Titer_{Max\ Titer} \cdot Harvest\ Yield_{Cell\ Debris}}{T} = \frac{Titer_{Max\ Density} \cdot Harvest\ Yield_{No\ Cell\ Debris}}{T - x}$$

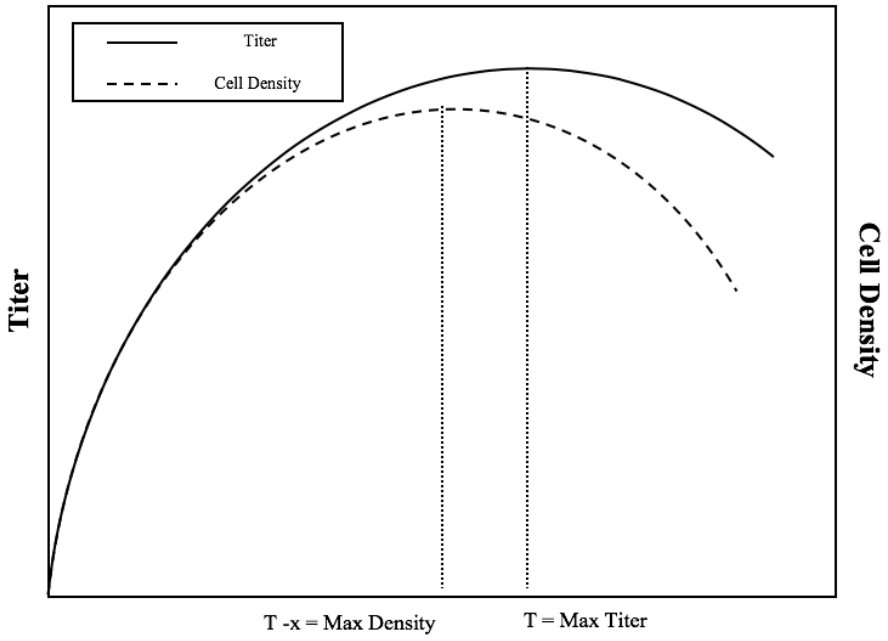

Figure 4-4. Cell Density versus Titer Trade-off. *Titer in the production bioreactor continues to increase after the cell density has decreased. The decrease in cell density implies decreased cell viability and increased cell debris.*

From the model (**Table 4-3**), harvest yield with and without 1 µm cell debris is 78% and 96.31%, respectively (note that these values do not account for flux interactions). After plugging in these values and rearranging terms, the calculation becomes (**Eq. 4-11**):

$$\left(1 - \frac{96.31\% \cdot Titer_{Max\ Density}}{78\% \cdot Titer_{Max\ Titer}}\right) \cdot T = x$$

From **Eq. 4-11**, harvest should be shifted earlier if the reduction in titer is outweighed by the combined effects of 1) the increase in harvest yield due to reduction in large cell debris and 2) the reduction in the duration of the production bioreactor step (x). Because the production bioreactor is the rate-limiting step, the reduced duration enables more turnover and thus increases capacity: 18.25 batches can be completed per year with a 20-day production bioreactor duration (T), while 24.33 batches can be completed per year with a 15-day duration (back-of-the-envelope calculation; excluded maintenance days, etc.). **Figure 4-5** illustrates the conditions at which it is beneficial to harvest earlier for various production bioreactor durations.

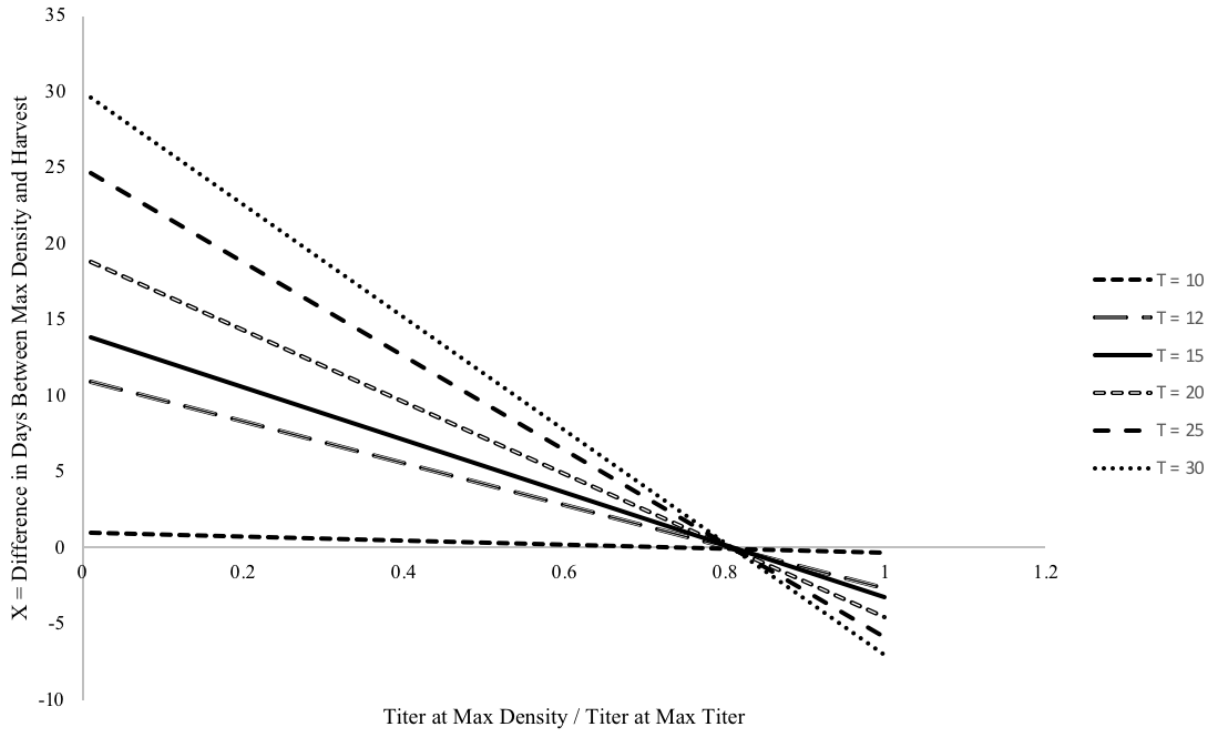

Figure 4-5. Delta Titer versus Delta Production Bioreactor Duration. *The figure plots the conditions at which it is beneficial to harvest earlier. If the titer at max cell density is significantly lower than max titer, then the duration must be significantly reduced to compensate for the decreased titer with increased turnover.*

Eq. 4-11 maximizes harvest yield per unit time but does not consider economics. Production capacity increases with increased harvest yield per unit time. Consequently, Amgen is able to fulfill high patient demand and increase its revenues. However, the direction of the costs is uncertain. Labor costs per gram of product will decrease because more product is produced within a given time period. But, the more frequent changeover adds material costs – e.g., additional media and filters. Thus, shifting harvest earlier to maximize harvest yield per time will only be economically beneficial if: 1) the decrease in labor costs outweighs the increase in material costs; 2) the decrease in labor costs does not outweigh the increase in material costs, but the additional revenue compensates for any increase in costs (which is probable because drug prices are notably higher than production costs).

Though shifting harvest earlier is a seemingly "simple" solution to reduce fouling, the complex economics pose uncertainties. Thus, Amgen should also investigate harvest equipment that reduces shear and/or genetically engineering cells to increase viability. Moreover, maximizing titer is an engrained philosophy at many biotech companies. Refocusing to maximum the harvest yield based on the trade-off of cell viability and titer will require a change in mindset. Because many biotechnology companies are data drive, the push to consider cell viability may happen easily if the numbers support it.

vi. Fraction <0.1 μm

The <0.1 μm fraction is analyzed separately because, as exhibited in **Figure 4-3**, this particle size fraction is a clear outliner. All other particle size groups follow the expected trend where larger particle sizes are associated with a linear increase in fouling, as measured by a linear increase in TMP and linear decrease in sieving and harvest yield. However, the <0.1 μm fraction deviates from this trend – instead of exhibiting minimal fouling, it is associated with the highest average TMP and lowest average sieving

and harvest yield. To evaluate the significance of the findings, the data was fit to the following model, which treats the particle size fractions as independent variables to discern the impact of each fraction (**Eq. 4-12**):

$$A \cdot Pore\ Size + B \cdot Flux + C \cdot Fraction1 + D \cdot Fraction\ 2 + E \cdot Fraction3 + F \cdot Fraction4 + G \cdot Fraction5 + H \cdot Fraction6 = Response$$

The model fit is displayed in **Table 4-4**. Fraction <0.1 µm is associated with significant fouling compared to the other particle size fractions. For example, Fraction <0.1 µm is associated with a 38.11% decrease in harvest yield from the intercept, while Fraction 0.1-0.22 µm is associated with a 19.83% increase in harvest yield from the intercept (intercept = 74.79%). Importantly, Fraction 0.1-0.22 µm *does not improve* harvest yield – it is associated with a suboptimal harvest yield (<100%). However, compared to Fraction <0.1 µm, Fraction 0.1-0.22 µm is associated with less fouling and higher harvest yields.

	TMP		Sieving		Harvest	
Summary of Fit	**Value**	**p-value**	**Value**	**p-value**	**Value**	**p-value**
R-square Adj	0.6975	N/A	0.7352	N/A	0.7620	N/A
F-ratio	**14.8356**	**<0.0001***	**17.6626**	**<0.0001***	**20.2056**	**<0.0001***
Parameter	**Value**	**p-value**	**Value**	**p-value**	**Value**	**p-value**
Intercept (psi)	-1.5198	0.1652	0.7366	**<0.0001***	**0.7479**	**<0.0001***
Pore Size (psi/µm)	-0.0726	0.9781	0.1733	0.2696	0.1439	0.2528
Flux (psi/LMH)	**0.5677**	**<0.0001***	**-0.0116**	**0.0299***	**-0.0134**	**0.0024***
Particle Size < 0.1 µm (binary)	**3.0232**	**<0.0001***	**-0.4214**	**<0.0001***	**-0.3811**	**<0.0001***
Particle Size 0.1-0.22 µm (binary)	**-3.3273**	**0.0003***	**0.2711**	**<0.0001***	**0.1984**	**<0.0001***
Particle Size 0.22-0.45 µm (binary)	**-1.7299**	**0.0352***	**0.1257**	**0.0105**	**0.1189**	**0.0030***
Particle Size 0.45-0.65 µm (binary)	**-2.1035**	**0.0161***	**0.1952**	**0.0003***	**0.1602**	**0.0002***
Particle Size 0.65-1 µm (binary)	0.5393	0.5455	-0.0239	0.6492	-0.0115	0.7878

Table 4-4. Model Results (Independent Fractions). *The table shows the results of fitting the empirical data (excluding Fraction <0.1 µm) to the following model:* A·Pore Size + B·Flux + C·Fraction1 + D·Fraction2 + E·Fraction3 + F·Fraction4 + G·Fraction5 + F·Fraction6 = Response Variable*. The bolded coefficients and starred p-values are statistically significant at an alpha of <0.05. The model fit shows that Fraction1 is associated with significant fouling compared to the other particle size fractions.*

Fraction <0.1 µm is associated with significant fouling across all operating conditions. Most surprisingly, the fraction is associated with fouling even when using a large pore size. Given that the pore size is over 4x the particle size, one would expect the small particles to readily pass through the filter. However, as indicated by the steep rise in TMP (**Figure 4-6**), the particles cause rampant fouling instead of easily permeating the filter.

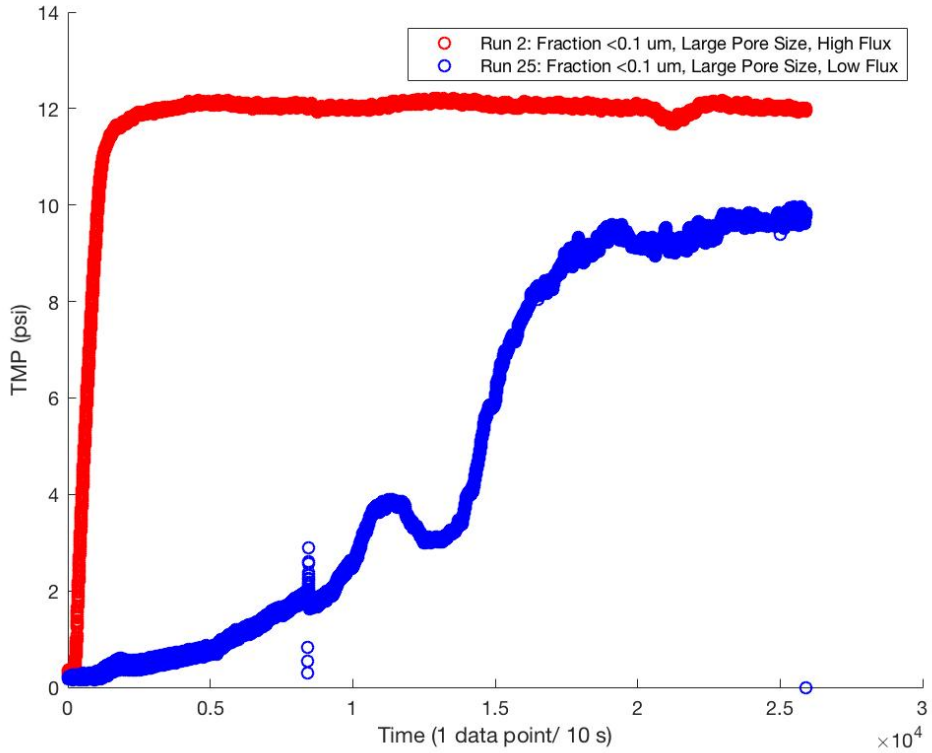

Figure 4-6. TMP Curves for Run 2 and Run 25. *The figure displays two TMP curves. Both Run 2 and 25 were filtered with <0.1 µm particles and large pores. The TMP increased rapidly for both runs, indicating rampant fouling.*

The results of Fraction <0.1 μm suggest that particle size is partially confounded by other variables – e.g., particle chemistry or shape. If particle size was the only factor, one would expect Fraction <0.1 μm to exhibit minimal fouling, in line with the other particle size fractions. However, because Fraction <0.1 μm exhibits significant fouling, other factors are likely at play. Possible reasons the smallest particles exhibit the most fouling include:

- <0.1 μm particles aggregate with each other (or the product), forming larger complexes that cannot pass through the filter pores.
- <0.1 μm particles are strongly attracted to the membrane surface, and thus form cake layers or block filter pores.

Cell culture additives, such as antifoam, may also have contributed to the rampant fouling exhibited by Fraction <0.1 μm. Because the supernatant was fractionated using a series of filters, antifoam and other additives permeate the filters and accumulate in the last fraction: Fraction <0.1 μm. Antifoam has been shown to foul membranes [43] and hence may have caused fouling in the runs with particles <0.1 μm.

The unexpected findings warrant further analysis of Fraction <0.1 μm. If the analysis identifies antifoam as the primary culprit, the concentration of antifoam should be reduced to maximize harvest yield. If the analysis instead determines the particles alone cause fouling, the particles should be eliminated via pre-filtration. Based on the results, the elimination of the minute particles – either via minimizing antifoam or pre-filtration – would increase harvest yield by up to 38.11% (**Table 4-4**).

C. Step 3: Polystyrene Microspheres Filtered using TFF

Polystyrene microspheres were also filtered using TFF to elucidate the importance of particle size versus other particle characteristics: e.g., chemistry and shape. The polystyrene microspheres were of similar size to two particle size fractions that exhibited rampant fouling: Fraction <0.1 μm and Fraction 0.65-1 μm. Moreover, the microspheres were filtered under conditions that exhibited significant fouling for these particle sizes (**Table 4-5)**.

Pair Number	Supernatant Condition	Microsphere (MS) Condition
1	Particle Size: 0.65 – 1 μm Pore Size: 0.45 μm Permeate Flux: 9 LMH	MS Size: 1 μm Pore Size: 0.45 μm Permeate Flux: 9 LMH
2	Particle Size: < 0.1 μm Pore Size: 750 kDa Permeate Flux: 9 LMH	MS Size: 0.1 μm Pore Size: 750 kDa Permeate Flux: 9 LMH

Table 4-5. Microsphere Operating Conditions. *Microspheres were filtered under the same conditions as supernatant of the corresponding particle size. Microspheres served as a control – allowing the differentiation between particle size and chemistry.*

The data suggests that filtering microspheres results in minimal fouling. While both supernatant conditions are associated with steep increases in TMP, the TMP remained around 0 psi while filtering microspheres (**Figure 4-7 A and B**). Moreover, the sieving and harvest yield remained greater than 75% for both runs using microspheres, while sieving and harvest yield was less than 60% for both supernatant runs (**Table 4-6**). A two-sample t-test shows that the fouling data using microspheres and supernatant arises from distinct distributions (p-value < 0.0001*).

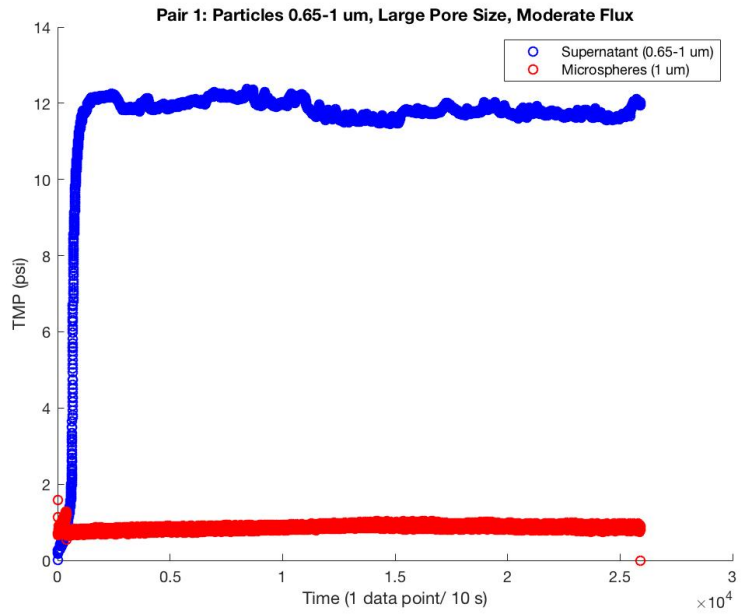

Figure 4-7A. Microsphere vs. Supernatant (Pair 1)*. The TMP data is shown for supernatant (0.65-1 µm particles, large pore sizes, moderate flux) and microspheres (1 µm MS, large pore sizes, moderate flux). The TMP rapidly rose for the supernatant but remained steady for the microspheres.*

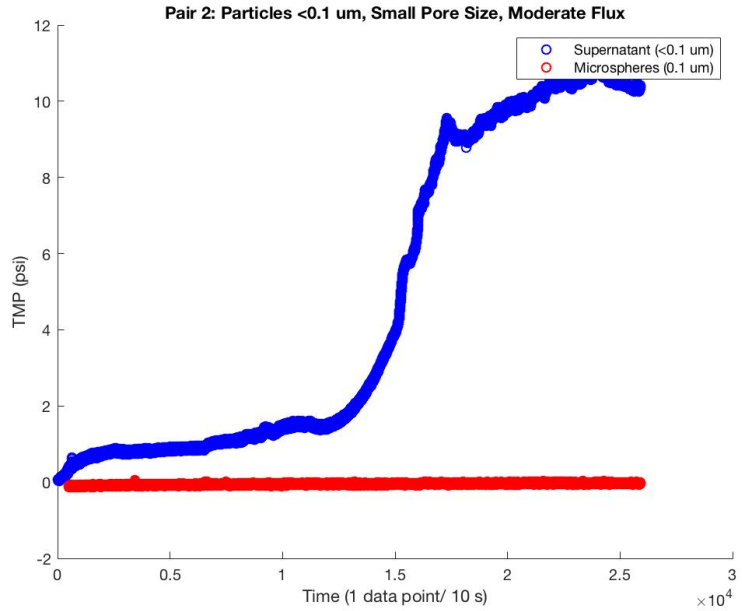

Figure 4-7B. Microsphere vs. Supernatant (Pair 1)*. The TMP data is shown for supernatant (<0.1 µm particles, small pore sizes, moderate flux) and microspheres (0.1 µm MS, small pore sizes, moderate flux). The TMP rapidly rose for the supernatant but remained steady for the microspheres.*

	TMP		Sieving		Harvest	
Pair	**Supernatant**	**Microspheres (MS)**	**Supernatant**	**Microspheres (MS)**	**Supernatant**	**Microspheres (MS)**

1 0.65-1 μm Large Pore Size Moderate Flux	11.54	0.8695	0.1818	0.7705	18.32%	76.23%
2 <0.1 μm Small Pore Size Moderate Flux	4.69	-0.247	0.5050	1.006	58.36%	87.66%

Table 4-6. Microspheres vs. Supernatant. *Microspheres were filtered under similar conditions to the supernatant to compare their fouling profiles and elucidate the importance of particle size versus other particle characteristics: e.g., chemistry and shape.*

If size was the only particle characteristic that influenced fouling, one would expect the microspheres to exhibit similar fouling profiles as supernatant. Thus, the differences between the microspheres and supernatant suggest that particle size is not the sole factor influencing fouling. Other factors contributing to fouling include particle chemistry and shape. Unless chemically modified, polysulfone (PS) membranes are hydrophobic [40]. Consequently, hydrophobic cellular components – e.g., lipids and proteins – are likely attracted to the membrane surface, explaining the observed differences between the supernatant and microspheres. Moreover, DNA likely adheres to the membrane surface. Massie *et al.* demonstrated that the addition of DNase I reduced fouling, suggesting that DNA contributes heavily to fouling [44].

Together, the particle size fraction and microsphere results demonstrate that both particle size and chemistry influence the extent of fouling. All supernatant fractions likely contained hydrophobic components that increased adhesion to the membrane surface. With the exception of Fraction <0.1 μm, larger particles more readily fouled the membrane surface than smaller particles because of their larger surface area. The larger surface area increases the drag forces on the particles due to permeate flow – according to Stoke's Law, drag forces increase with radius (**Eq. 4-13):**

$$F_D = 6\pi\mu R v \Omega$$

, where Ω is Happel's correction factor for crossflow) [41]. The larger hydrophobic surface area also likely increases "adhesion area" and the amount of membrane covered by a deposited particle. To minimize fouling from hydrophobic components, polysulfone membranes can be chemically modified to minimize their hydrophobicity [40].

Chapter 5: Conclusion

Many biotechnology companies are moving from fed-batch to perfusion cell culture. Perfusion processes enable higher cell density and productivity compared to fed-batch, allowing for smaller manufacturing facilities and lower capital investment. However, many traditional harvest technologies cannot support the high cell densities achieved with perfusion culture while maintaining a small manufacturing footprint. Microfiltration-based tangential flow filtration (TFF) and alternating tangential flow filtration (ATF) best support the high cell densities but readily foul, leading to low harvest yield. Thus, there is a need to understand what causes fouling and how to reduce it.

Through a series of filtration experiments using fractionated supernatant, we showed that both particle size and flux are associated with fouling and low harvest yield. Except for particles <0.1 um, increasing the particle size was associated with an increase in fouling. Particles <0.1 um were an outlier – though they were the smallest particles tested, they resulted in severe fouling likely because of aggregation or high antifoam concentration. Pore size, surprisingly, was not associated with fouling, suggesting that caking is the primary mode of fouling.

We also filtered polystyrene microspheres that were of similar sizes to the supernatant. The microspheres did not exhibit the same fouling profile as the particle size fractions, suggesting that size is not the only determinant of fouling. Both particle size and chemistry influence the extent of fouling.

Amgen Proprietary - Confidential

Based on the results, to increase the robustness of harvest, problematic cell debris should be reduced before harvest and the permeate flux should be decreased. Two particle size bands proved to be the most problematic – large particles ~1 μm and small particles less than 0.1 μm. Possible solutions to reduce large cell debris include engineering cells with higher viability, pre-filtering the feed solution, reducing shear from the pump, and shifting harvest earlier. Possible solutions to reduce the small cell debris are reducing the antifoam concentration (a potential culprit underlying these particles) and pre-filtrating the feed solution.

The project implications cut across all product lines – providing insights into methods that may improve harvest yield regardless of the product. Continued initiatives that are agnostic to product lines are recommended because the results may drastically impact the overall manufacturing approach and capacity. Sharing of learnings across product-specific projects can have a similar affect – acquired knowledge is often translatable across the product lines.

Bibliography

[1] G. Walsh, *Pharmaceutical biotechnology: Concepts and Applications*. John Wiley & Sons, Ltd., 2007.

[2] M. Mikulic, "Biotechnology industry - Statistics & Facts," *statista*, 2018. [Online]. Available: https://www.statista.com/topics/1634/biotechnology-industry/. [Accessed: 19-Sep-2019].

[3] R. A. Bradway, "Amgen CEO Letter to Stakeholders," 2018.

[4] J. Pollock, S. V. Ho, and S. S. Farid, "Fed-batch and perfusion culture processes: Economic, environmental, and operational feasibility under uncertainty," *Biotechnol. Bioeng.*, vol. 110, no. 1, pp. 206–219, 2013.

[5] W. Kelly *et al.*, "Understanding and modeling alternating tangential flow filtration for perfusion cell culture," *Biotechnol. Prog.*, vol. 30, no. 6, pp. 1291–1300, 2014.

[6] S. Wang, S. Godfrey, J. Ravikrishnan, H. Lin, J. Vogel, and J. Coffman, "Shear contributions to cell culture performance and product recovery in ATF and TFF perfusion systems," *J. Biotechnol.*, vol. 246, pp. 52–60, 2017.

[7] T. C. Dickenson, *Filters and Filtration Handbook*. Elsevier, 1997.

[8] R. W. Field, D. Wu, J. A. Howell, and B. B. Gupta, "<Field et al._Critical Flux Concept for Microfiltration Fouling.pdf>," vol. 100, pp. 259–272, 1995.

[9] A. F. Jozala *et al.*, "Biopharmaceuticals from microorganisms: from production to purification," *Brazilian J. Microbiol.*, vol. 47, pp. 51–63, 2016.

[10] T. Lai, Y. Yang, and S. K. Ng, "Advances in mammalian cell line development technologies for recombinant protein production," *Pharmaceuticals*, vol. 6, no. 5, pp. 579–603, 2013.

[11] J. Dumont, D. Euwart, B. Mei, S. Estes, and R. Kshirsagar, "Human cell lines for biopharmaceutical manufacturing: history, status, and future perspectives," *Crit. Rev. Biotechnol.*, vol. 36, no. 6, pp. 1110–1122, 2016.

[12] T. Hernández Rodríguez, R. Pörtner, and B. Frahm, "Seed train optimization for suspension cell culture," *BMC Proc.*, vol. 7, no. Suppl 6, p. P9, 2013.

[13] The Northeast Biomanufacturing Center and Collaborative, "Introduction to Biomanufacturing - Downstream Processing Chapter 11," 2016.

[14] F. Li, N. Vijayasankaran, A. Shen, R. Kiss, and A. Amanullah, "Cell culture processes for monoclonal antibody production," *MAbs*, vol. 2, no. 5, pp. 466–479, 2010.

[15] S. M. Woodside, B. D. Bowen, and J. M. Piret, "Mammalian cell retention devices for stirred perfusion bioreactors," *Cytotechnology*, vol. 28, no. 1–3, pp. 163–175, 1998.

[16] A. S. Jerry Shevitz, John Bonham-Carter, Janice Lim, PhD, "An Economic Comparison of Three Cell Culture Techniques," *BioPharm Int.*, vol. 24, no. 2, 2011.

[17] C. L.R. and M. R.A., "Cell Retention Devices for Suspended-Cell Perfusion Cultures," *Tools Appl. Biochem. Eng. Sci.*, vol. 74, pp. 129–169.

[18] D. J. Karst, E. Serra, T. K. Villiger, M. Soos, and M. Morbidelli, "Characterization and comparison of ATF and TFF in stirred bioreactors for continuous mammalian cell culture processes," *Biochem. Eng. J.*, vol. 110, pp. 17–26, 2016.

[19] K. RM, "Expanded-bed adsorption chromatography.," *Curr Protoc Protein Sci*, vol. 8, no. 8, 2005.

[20] M. Iqbal *et al.*, “Aqueous two-phase system (ATPS): an overview and advances in its applications,” *Biol. Proced. Online*, vol. 18, no. 1, pp. 1–18, 2016.
[21] J. A. Asenjo and B. A. Andrews, “Aqueous two-phase systems for protein separation: A perspective,” *J. Chromatogr. A*, vol. 1218, no. 49, pp. 8826–8835, 2011.
[22] A. Drews, “Membrane fouling in membrane bioreactors-Characterisation, contradictions, cause and cures,” *J. Memb. Sci.*, vol. 363, no. 1–2, pp. 1–28, 2010.
[23] B. Kruczek, “Encyclopedia of Membranes,” *Encycl. Membr.*, pp. 1–3, 2015.
[24] F. Radoniqi, H. Zhang, C. L. Bardliving, P. Shamlou, and J. Coffman, “Computational fluid dynamic modeling of alternating tangential flow filtration for perfusion cell culture,” *Biotechnol. Bioeng.*, vol. 115, no. 11, pp. 2751–2759, 2018.
[25] K.-V. Peinemann and S. P. Nunes, *Membranes for Water Treatment*, 4th ed. .
[26] C. Taddei, P. Aimar, J. A. Howell, and J. A. Scott, “Yeast cell harvesting from cider using microfiltration,” *J. Chem. Technol. Biotechnol.*, vol. 47, no. 4, pp. 365–376, 1990.
[27] S. Sablani, M. Goosen, R. Al-Belushi, and M. Wilf, “Concentration polarization in ultrafiltration and reverse osmosis: A critical review,” *Desalination*, vol. 141, no. 3, pp. 269–289, 2001.
[28] V. Chen, A. G. Fane, S. Madaeni, and I. G. Wenten, “Particle deposition during membrane filtration of colloids: Transition between concentration polarization and cake formation,” *J. Memb. Sci.*, vol. 125, no. 1, pp. 109–122, 1997.
[29] G. R. Bolton and A. J. Apostolidis, “Mechanistic modeling of the loss of protein sieving due to internal and external fouling of microfilters,” *Biotechnol. Prog.*, vol. 33, no. 5, pp. 1323–1333, 2017.
[30] C. Duclos-Orsello, W. Li, and C. C. Ho, “A three mechanism model to describe fouling of microfiltration membranes,” *J. Memb. Sci.*, vol. 280, no. 1–2, pp. 856–866, 2006.
[31] B. Ladewig and M. N. Z. Al-Shaeli, *Fundamentals of Membrane Bioreactors*. .
[32] Hermia, “Paper 42.pdf.” .
[33] M. F. Clincke, C. Möller yd, Y. Zhang, E. Lindskog, K. Walsh, and V. Chotteau, “Very high density of CHO cells in perfusion by ATF or TFF in WAVE bioreactor™: Part I: Effect of the cell density on the process,” *Biotechnol. Prog.*, vol. 29, no. 3, pp. 754–767, 2013.
[34] Y. Marselina, Lifia, P. Le-Clech, R. M. Stuetz, and V. Chen, “Characterisation of membrane fouling deposition and removal by direct observation technique,” *J. Memb. Sci.*, vol. 341, no. 1–2, pp. 163–171, 2009.
[35] M. Stressmann and C. Moresoli, “Effect of pore size, shear rate, and harvest time during the constant permeate flux microfiltration of CHO cell culture supernatant,” *Biotechnol. Prog.*, vol. 24, no. 4, pp. 890–897, 2008.
[36] S. B. Wang, S. Godfrey, F. Radoniqi, H. Lin, and J. Coffman, “Larger Pore Size Hollow Fiber Membranes as a Solution to the Product Retention Issue in Filtration-Based Perfusion Bioreactors,” *Biotechnol. J.*, vol. 14, no. 2, 2019.
[37] R. T. Anthony Atkinson, Alexander Donev, *Optimum Experimental Designs, with SAS (Oxford Statistical Science Series)*. Oxford University Press, 2007.
[38] Levitronix, “Pumps for Ultra Pure Fluidhandling.” [Online]. Available: https://www.levitronix.com/en/home.html.
[39] Roche Diagnostics, “Cedex Bio HT Analyzer.” [Online]. Available: https://custombiotech.roche.com/home/Product_Details/INS_3590.html.
[40] H. T. V. Nguyen *et al.*, “Preparation and characterization of a hydrophilic polysulfone

membrane using graphene oxide," *J. Chem.*, vol. 2019, pp. 15–20, 2019.
[41] J. C. Chen, M. Elimelech, and A. S. Kim, "Monte Carlo simulation of colloidal membrane filtration: Model development with application to characterization of colloid phase transition," *J. Memb. Sci.*, vol. 255, no. 1–2, pp. 291–305, 2005.
[42] J. Y. Kim, Y. G. Kim, and G. M. Lee, "CHO cells in biotechnology for production of recombinant proteins: Current state and further potential," *Appl. Microbiol. Biotechnol.*, vol. 93, no. 3, pp. 917–930, 2012.
[43] J. Lecomte and DOW, "The Effects of Antifoams on Ultrafiltration Membranes," p. 5, 2012.
[44] S. Mercille, M. Johnson, R. Lemieux, and B. Massie, "Filtration-based perfusion of hybridoma cultures in protein-free medium: Reduction of membrane fouling by medium supplementation with DNase I," *Biotechnol. Bioeng.*, vol. 43, no. 9, pp. 833–846, 1994.
[45] B. D. Perlman, "[7] U s e o f A n t i b i o t i c s in Cell C u l t u r e M e d i a itations for their use , and the practical value of this strategy . The basic requirements are : 1 . The antibiotic must eliminate the microbial contaminant . (Bacteri- cidal compounds," vol. LVIII, no. 2, pp. 110–116, 1962.

Appendices

Appendix A: Multivariate Analysis

When scoping the project, partial-least squares (PLS) regression was conducted to assess which factors best predict harvest yield. PLS is a method for building predictive models when there are many colinear factors. The goal of PLS is the use the factors to predict the responses in the population. This is achieved by extracting latent variables T (X-scores) and U (Y-scores) from the factors and responses, respectively. The X-scores are used to predict the Y-scores, and the Y-scores are then used to predict the responses (**Figure Appendix-1**).

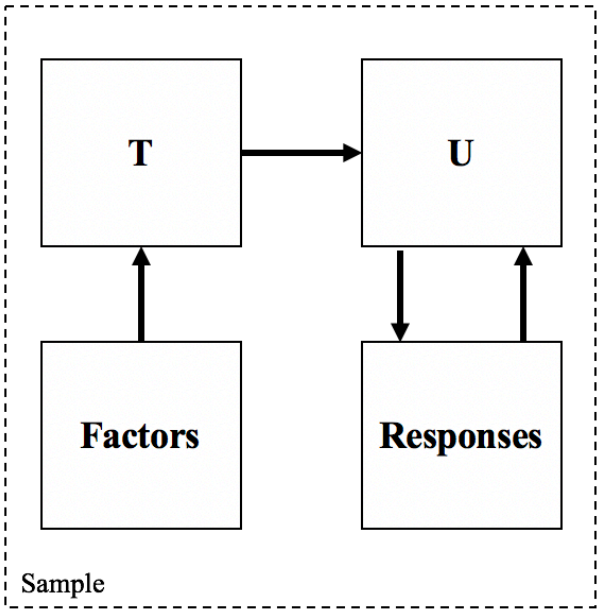

Figure Appendix-1. Partial Least Squares Regression Methodology. *Latent variables are extracted from the factors and are used to predict the responses.*

The multivariate analysis was conducted on Amgen Pilot Lab data – fifty-seven filtration runs in total. Forty factors were measured and recorded during the filtration runs, including data on the filter, TMP,

and cell viability. The forty factors were mapped to two response variables (average sieving and yield) using PLS. The resulting model extracted two latent variables, which heavily weighted low TMP, large filter pore sizes, and turbidity (indicating that these variables are positively correlated with average sieving and yield). The following factors were negatively weighted when constructing the latent variables, suggesting that they are negatively correlated with average sieving and yield: higher flux, smaller pore size, and titer.

Overall, the model did not fit nor predict the response variables well. The R^2, or percent variation of the training set explained by the model, was ~ 0.5. The Q^2, or percent variation of the training set predicted by the model via cross-validation, was <0.5. The poor performance of the model is likely because there was little variation in the factors across the fifty-seven filtration runs. Despite the performance, the PLS model supported varying flux and filter poor size in addition to particle size because these factors seem to be highly correlated with sieving and yield.

Appendix B: Loading Experiment

75 mL of the particle size fraction (supernatant) was added to the main container. The volume of supernatant was determined via a series of loading experiments. The goal of the loading experiments was to determine the smallest loading (main container volume / filtration area) necessary to achieve typical fouling profiles. When filtering cell culture with moderate permeate flux and moderately-sized pores, Amgen typically observes a rapid increase in TMP. In contrast, when filtering cell culture with low permeate flux and moderately-sized pores, Amgen typically observes no increase in TMP over the three-day harvest. These observations served as the standards against which the loading experiment results were compared.

A small loading volume was desired given material constraints. The output of Step 1 was ~1 L of each particle size fraction; 1 L of supernatant divided by 9 conditions is 0.111 L of supernatant per filtration run. Given a filtration area of 0.0038 m^2 (see **Chapter 3, Section 3, "Microfiltration polysulfone cartridges"**), 0.111 L of supernatant translates to a loading of 29.211 L/m^2. If accounting for four to five reruns per fraction, 75 mL of supernatant, or 19.737 mL/m^2, is necessary per filtration run. Thus, 19.737 mL/m^2 became the first loading tested in the loading experiments. Note that this is approximately 1/10 of the typical loading used in production.

The feed solution for the loading experiments was un-fractionated supernatant (i.e., supernatant with all particle sizes). The filtration set-up was similar to the set-up pictured in **Figure 3-6**, with the exception that the bearingless pump was replaced with a peristaltic pump. With a loading volume of 19.737 mL/m^2, filtered using a membrane with 0.45 μm pores, a steep increase in TMP was seen with moderate flux (9 LMH) while no increase in TMP was seen with low flux (4.5 LMH). These results match the typical TMP profiles, and thus the loading volume of 19.737 mL/m^2 is representative of higher loading volumes. 19.737 mL/m^2, or 75 mL of supernatant, was used for all runs in the DOE.

Appendix C: Antibiotic Experiments

When selecting the antibiotic, two criteria were evaluated: the antibiotic must 1) prohibit further breakdown of cell debris within the supernatant, which would distort the particle size analysis, and 2) prevent both gram-positive and gram-negative bacteria. Penicillin-streptomycin fulfilled both criteria. Penicillin-streptomycin is nontoxic and safe to mammalian cells [45]; we infer that if an antibiotic is safe for viable cells, it will not disrupt cell debris.

Penicillin-streptomycin was purchased from Sigma-Aldrich. The solution contained 10,000 units of penicillin and 10 mg of streptomycin per mL. The recommended dosage is 10 mL of Penicillin-streptomycin solution per liter of culture. Given 75 mL of supernatant per run, 0.75 mL of antibiotic solution is required per run. Before conducting the DOE, the dosing frequency was confirmed by adding antibiotic solution to un-fractionated supernatant at room temperature. After adding antibiotics, a sample of the supernatant was examined under a microscope once per day for three days. No bacterial growth was observed over three days. Hence, one dose of antibiotics (0.75 mL) at the start of each filtration run is sufficient to prevent contamination.

Appendix D: Additional Variables

The following variables were also a potential source of variation and were iteratively incorporated into the model. However, none were evaluated to be statistically significant:

- Run Number: Adding "Run Number" as an independent variable would capture any systematic variability due to the learning curve of setting-up and running the experiments. However, the "Run Number" coefficient was not statistically significant (p-value > 0.1), likely because the DOE already accounted for the learning curve by randomizing the run order.
- Peristaltic Pump Number/Levitronix Pump Number: Adding "Pump Number" as an independent variable would capture equipment differences, such as different crossflow rates or permeate fluxes given the same input. Incorporating "Pump Number" did not improve the fit of the model and the coefficient was statistically insignificant (p-vale > 0.1). The lack of

significance suggests that there were no glaring differences between the pumps – likely because of the routine calibration (the pumps were re-calibrated every three weeks).

- Filter Batch Number: Previously, Amgen identified large differences in quality between filter batches. The manufacturer has since improved its manufacturing processes and no significant differences between filter batches were seen (p-value of "Batch Number" coefficient = > 0.1).